METABOLIC REGULATION OF PROTEIN PHOSPHORYLATION AND ACETYLATION

APPROVED BY SUPERVISORY COMMITTEE

Benjamin P. Tu, Ph.D.

Jennifer J. Kohler, Ph.D.

Deepak Nijhawan, M.D., Ph.D.

Hongtao Yu, Ph.D.

DEDICATION

To my parents for their love and support.

To my mentor and committee members for their guidance.

METABOLIC REGULATION OF PROTEIN PHOSPHORYLATION AND ACETYLATION

by

MENGLU ZHANG

DISSERTATION

Presented to the Faculty of the Graduate School of Biomedical Sciences

The University of Texas Southwestern Medical Center at Dallas

In Partial Fulfillment of the Requirements

For the Degree of

DOCTOR OF PHILOSOPHY

The University of Texas Southwestern Medical Center at Dallas

Dallas, Texas

August, 2018

METABOLIC REGULATION OF PROTEIN PHOSPHORYLATION AND ACETYLATION

Menglu Zhang

The University of Texas Southwestern Medical Center at Dallas, 2018

Supervising Professor: Benjamin P. Tu, Ph.D.

Celluar metabolism can influence phosphorylation and acetylation modifications on proteins as part of an intricate network of cellular and organismal regulation. We have investigated one molecular mechanism through which protein phosphorylation and acetylation can be regulated based on metabolic status and how metabolic enzymes are regulated by nutrient availability.

In the first part of this study, we report that a simple enzyme involved in acetate utilization, Acetyl-CoA synthetase 2 (ACSS2), promotes systemic fat storage and utilization through selective regulation of genes involved in lipid metabolism. We reveal that mice

lacking ACSS2 exhibit a significant reduction in body weight and hepatic steatosis in a diet-induced obesity model. ACSS2 deficiency reduces dietary lipid absorption by the intestine, and perturbs repartitioning and utilization of triglycerides from adipose tissue to the liver due to lowered expression of lipid transporters and fatty acid oxidation genes. In this manner, ACSS2 promotes the systemic storage or metabolism of fat according to the fed or fasted state. Targeting ACSS2 may therefore offer therapeutic benefit for the treatment of fatty liver disease.

We also report that ACSS2 may play a critical role in the development of pancreatic cancer. We have demonstrated that ACSS2 expression in a KRas-driven mouse model of pancreatic ductal adenocarcinoma (PDAC) showed that ACSS2 was absent in normal pancreatic tissue but expressed at very high levels in precancerous lesions of PDAC. The absence of ACSS2 in mouse pancreatic cancer models reduced the tumor burdens, and ACSS2 expression is correlated with tumor size. These data indicate that ACSS2 has a potential function in the development of PDAC. The experiments reported in the first two chapters of this thesis were performed in close collaboration with a former postdoc in the lab, Dr. Zhiguang Huang.

In the second part of the study, we report that methylation of Protein Phosphatase 2A (PP2A) may play a critical role in regulating cell growth and autophagy. We have reconstituted the methylation activity of leucine carboxyl methyltransferase 1 (LCMT-1) *in vitro* and determined the kinetic parameters of LCMT-1-catalyzed methylation of PP2A. We reveal that LCMT-1 might be a “SAM sensor” as it is very sensitive to the SAM/SAH ratio. Methionine deprivation study in cell lines revealed that methionine depletion boosts PP2A

demethylation. We further conducted a high-throughput screen to identify potent and specific small molecule inhibitors of LCMT-1.

Table of Contents

List of Figures

CHAPTER 1

List of Tables

List of Definitions

ACAA1 – acetyl-CoA acyltransferase 1

Acetyl-CoA – acetyl coenzyme A

ACLY – ATP citrate lyase enzyme

ACOX1 – peroxisomal acyl-coenzyme A oxidase 1

ACS – acetyl-CoA synthetase

ACSS2 – Acetyl-CoA synthetase 2

BSA – bovine serum albumin

BW – body weight

CD36 – cluster of differentiation 36

DBP – D site of albumin promoter binding protein

DGAT1 – diglyceride acyltransferase 1

DGAT2 – diglyceride acyltransferase 2

DHCR24 – 24-Dehydrocholesterol reductase

DMSO – dimethyl sulfoxide

DNMT1 – DNA methyltransferase 1

EHHADH – enoyl-CoA, hydratase/3-hydroxyacyl CoA dehydrogenase

epWAT – epididymal white adipose tissue

FA – fatty acid

FABP1 – liver fatty acid binding protein

FABP2 – intestine fatty acid binding protein

FAS – Fas cell surface death receptor

FATP4 – fatty acid transport protein 4

GEMM – genetically engineered mouse models

GO – gene ontology

GPAT1 – glycerol-3-phosphate acyltransferase 1

GTT – glucose tolerance test

H&E – haematoxylin and eosin

HCS – holocarboxylase synthetase

HCR – HMG-CoA reductase

HFD – high fat diet

HTS – high-throughput screen

IHC – Immunohistochemistry

IPMN – intraductal papillary mucinous neoplasm

ITC – isothermal titration calorimetry

ITT – insulin tolerance test

KAC – $Kras^{G12D}$; $Arid1a^{-/-}$; $p48^{Cre}$

KIC – LSL-$Kras^{G12D/+}$; $Cdkn2a^{Lox/Lox}$; $p48^{Cre}$

KO – knock out

KPC – LSL-$Kras^{G12D/+}$; LSL-$Trp53^{R172H/+}$; $Pdx\text{-}1^{Cre}$

KRAS – Kirsten Ras

LC-MS – liquid chromatography-mass spectrometry

LCMT-1 – leucine carboxyl methyltransferase 1

LSS – lanosterol synthase

LXR – liver X receptor

Met-PP2A – methylated PP2A

NAFLD – non-alcoholic fatty liver disease

NDP – nanozoomer digital pathology

NEFA – non-esterified fatty acid

NMR – nuclear magnetic resonance

Npr2p – natriuretic peptide receptor 2

OCT – optimal cutting temperature compound

ORO – oil red O

PanIN – pancreatic intraepithelial neoplasia

PBS – phosphate-buffered saline

PCR – polymerase chain reaction

PDAC – pancreatic ductal adenocarcinoma

PET – positron-emission tomography

PP2A – protein phosphatase 2A

PP2A-C – protein phosphatase 2A C subunit

PPARA – peroxisome proliferator-activated receptor alpha

PPARG – peroxisome proliferator-activated receptor gamma

PPM1 – protein phosphatase methyltransferase 1

RXR – retinoid X receptor

RXRA – retinoid X receptor alpha

SAM – S-adenosylmethionine

SAH – S-adenosylhomocysteine

SCD1 – Stearoyl-CoA desaturase-1

SCP2 – sterol carrier protein 2

SEM – standard error of the mean

SL – synthethic medium with lactate

SOX9 – sex determining region Y box 9

SREBP – sterol regulatory element-binding proteins

SREBP1 – sterol regulatory element-binding transcription factor 1

TCA – tricarboxylic acid

TG – triglycerides

TMA – tissue microarray

TORC1 – target of rapamycin complex 1

WAT – white adipose tissue

WT – wild type

CHAPTER ONE

Acetyl-CoA Synthetase 2 Promotes Systemic Fat Storage and Utilization Through Selective Regulation of Genes Involved in Lipid Metabolism

Introduction

ACSS2 (Acetyl-CoA synthetase 2) is a conserved nucleocytosolic enzyme that converts acetate to acetyl-CoA. It has been reported that adult mice lacking ACSS2 appear phenotypically normal but exhibit reduced tumor burdens in mouse models of liver cancer. However, the normal physiological functions of this alternate pathway of acetyl-CoA synthesis remain unclear. Here, we reveal that ACSS2 deficiency protects mice from obesity and hepatic steatosis in a diet-induced obesity model. ACSS2 deficiency reduces dietary lipid absorption by the intestine, and perturbs repartitioning and utilization of triglycerides from adipose tissue to the liver due to lowered expression of lipid transporters and fatty acid oxidation genes. Therefore, ACSS2 promotes the systemic storage or metabolism of fat according to the fed or fasted state. Targeting ACSS2 may offer therapeutic benefit for the treatment of fatty liver disease.

Acetyl-CoA and acetyl-CoA synthetase

Acetyl-CoA lies at the nexus of many pathways in central carbon metabolism (Shi and Tu, 2015). It is a key intermediate in the catabolism of carbohydrates and fats, which in turn fuels the mitochondrial TCA cycle. In parallel, it also serves as a two-carbon donor for the biosynthesis of fatty acids and sterols, which occurs in the cytosol. Two primary

pathways are involved in the generation of cytosolic acetyl-CoA. One is mediated by the ATP citrate lyase enzyme (ACLY) (Srere, 1959), which converts citrate exported from the mitochondria into acetyl-CoA for lipogenesis. Genetic deletion of Acly in mice results in embryonic lethality (Beigneux et al., 2004), suggesting the importance of this pathway as a primary generator of cytosolic acetyl-CoA.

Another pathway is contributed by the acetyl-CoA synthetase (ACS) family of enzymes (Jones et al., 1953; Berg, 1956), which are evolutionarily conserved from bacteria to mammals. Mice lacking ACSS2, the nucleocytosolic ACS, are viable and fertile (Comerford et al, 2014), consistent with the idea that it represents an alternative, non-essential pathway for cytosolic acetyl-CoA synthesis. Indeed, acetate, a common product of microbial fermentative metabolism, is not thought to be a major contributor to mammalian carbon metabolism due to its low concentrations in serum (Psychogios et al, 2011). However, mice lacking ACSS2 develop fewer tumors in two mouse models of hepatocellular carcinoma (Comerford et al, 2014), and many tumors are [^{11}C]acetate PET-positive (Grassi et al, 2012), suggesting the enzyme may supply a critical source of acetyl-CoA under specific conditions. Interestingly, substantial amounts of the enzyme are present in the nucleus (Comerford et al, 2014; Ariyannur et al, 2010), hinting that ACSS2 may play a role in the recapture of free acetate released from histone deacetylation (Comerford et al, 2014).

In this study, I sought to further understand the role of acetate and ACSS2 in normal physiology and metabolism. Mammalian ACSS2 was first cloned as a target of the SREBP transcription factors that regulate lipid homeostasis (Luong et al, 2000). By exposing mice to a high-fat diet or prolonged fasting, I helped discover that this simple metabolic enzyme

promotes the proper storage or utilization of fat according to the fed or fasted state. As such, ACSS2 has an unanticipated function in the control of systemic lipid metabolism through selective modulation of gene expression linked to acetate availability.

ACSS2 deletion protects against lipid deposition and obesity

To gain insight into the normal physiological function of ACSS2, we compared ACSS2-null mice to ACSS2+/+ and ACSS2+/- littermates fed a high-fat diet (HFD, 58.4% kcal from fat) or a standard diet (chow, 12% kcal from fat) starting at 9 weeks of age. On chow diet, there was no significant difference in body weight between genotypes over a period of ~12 weeks. On HFD, body weights were significantly lower in both male and female ACSS2-/- mice compared with ACSS2+/- or ACSS2+/+ mice (Figure 1.1). The reduced weight gain observed in ACSS2-/- mice was not due to reduced food consumption (Figure 1.2).

Under HFD conditions, the epididymal fat pads (epWAT) of ACSS2-/- mice were notably smaller compared to ACSS2+/+. Epididymal fat mass was also significantly lower in ACSS2-/- mice (Figure 1.3). NMR assessment of body composition further confirmed reduced total lipid content in ACSS2-/- mice (Figure 1.4). Adipocytes in epWAT of ACSS2-/- mice showed a reduction in size and decreased inflammatory infiltrates (Figure 1.5). Epididymal fat mass, body fat composition, epWAT size and inflammatory infiltration were not significantly different between ACSS2+/+ and ACSS2-/- mice fed a chow diet (Figure 1.6). Serum cholesterol, triglyceride, and phospholipid concentrations were each significantly decreased in ACSS2-/- mice fed a HFD (Figure 1.7), while no significant differences were

observed in ACSS2-/- mice fed a chow diet (Figure 1.8). Taken together, these results indicate that the absence of ACSS2 impedes fat deposition and obesity associated with high dietary fat intake.

ACSS2 deletion protects against hepatic steatosis

Insulin resistance and hepatic steatosis are two common pathological phenotypes associated with obesity. Under HFD conditions, we observed no significant differences in the levels of serum glucose and insulin between ACSS2+/+ and ACSS2-/- mice (Figure 1.9). Moreover, similar glucose clearance and insulin sensitivity were observed in ACSS2+/+ and ACSS2-/- mice (Figure 1.10). These results indicate that although ACSS2 deficiency might protect against obesity, it does not protect against the development of insulin resistance.

The majority of ACSS2+/+ animals developed moderate to severe hepatic steatosis under HFD conditions. Hepatic steatosis was significantly decreased in the majority of ACSS2-/- mice fed a HFD (Figure 1.11, 1.12). Liver mass and liver triglyceride accumulation were accordingly decreased in ACSS2-/- mice (Figure 1.13). Under chow diet conditions, ACSS2-/- livers were comparable to ACSS2+/+ livers in morphology and mass (Figure 1.14). We analyzed livers for expression of a panel of genes involved in lipid metabolism (Figure 1.15). The absence of ACSS2 was associated with decreased expression of“master”transcriptional regulators of lipid metabolism (PPARA, PPARG, SREBP1C) as well as key genes involved in fatty acid uptake and trafficking (CD36, FATP4, FABP1, FABP2), lipid synthesis (FAS, SCD1, HCS, HCR, DHCR24, LSS, GPAT1), and peroxisomal fatty acid oxidation (ACOX1, EHHADH, DBP, ACAA1, SCP2). Reduced

expression of these lipid metabolism genes likely accounts for decreased levels of triglyceride and lipids in circulation and in the liver. On chow diet, there was no significant difference in expression of genes involved in fatty acid uptake and transport between ACSS2+/+ and ACSS2-/- livers (Figure 1.16).

ACSS2 deletion reduces intestinal lipid absorption

We next evaluated intestinal lipid absorption as a possible mechanism for the reduced weight gain and hepatic steatosis noted in ACSS2-/- mice. Under HFD conditions, the length of the small intestine in ACSS2-/- mice was shorter compared with ACSS2+/+ mice (Figure 1.17). Although crypt number did not differ between genotypes, ACSS2-/- mice exhibited slightly shorter villi (Figure 1.18). Fecal lipid content was increased by ~25% in ACSS2-/- mice fed a HFD (Figure 1.19), but was not associated with a change in either stool color, consistency, output, or daily dietary lipid intake (Figure 1.20). In the fed condition on HFD, fewer and smaller lipid droplets were observed in the mucosa of the proximal intestine of ACSS2-/- mice (Figure 1.21). To investigate whether the reduction of lipid droplets in the intestine was due to reduction of lipid absorption, we fasted mice overnight and subjected them to olive oil gavage. Consistently, fewer and smaller lipid droplets were noted in the mucosa of the proximal intestine of ACSS2-/- mice after olive oil gavage compared with ACSS2+/+ mice (Figure 1.22).

Lipid absorption in the intestine is controlled by processes of fatty acid uptake and trafficking, triglyceride synthesis, droplet dynamics, chylomicron assembly and secretion (D'Aquila et al, 2016). We evaluated mRNA expression of panels of genes in each of these

processes in the small intestine as a function of ACSS2 genotype. Notably, FABP1, a major protein responsible for dietary lipid uptake (Storch and Corsico, 2008), and DGAT1 and DGAT2, principal enzymes in triglyceride synthesis (Yen et al, 2008), exhibited significantly reduced expression in the intestine of ACSS2-/- mice (Figure 1.23). Genes involved in droplet dynamics and chylomicron assembly and secretion did not show significant differences as a function of genotype (Figure 1.24). On chow diet, no difference was observed in expression of genes involved in dietary lipid uptake between ACSS2+/+ and ACSS2-/- small intestine (Figure 1.25). We confirmed by immunohistochemical staining that FABP1 protein levels were also reduced in the enterocytes of ACSS2-/- mice (Figure 1.26).

We then examined the distribution of ACSS2 protein in intestinal enterocytes and in cells of the intestinal crypt. ACSS2 was present in both nucleus and cytoplasm in the intestinal crypt. By contrast, in the enterocytes, ACSS2 was present predominantly in the nucleus. Notably, nuclear expression of ACSS2 in enterocytes was reduced in the chow diet and fasting conditions compared with the HFD condition (Figure 1.27). High nuclear ACSS2 protein abundance in enterocytes was correlated with increased expression of FABP1 and lipid absorption genes in HFD-fed mice. These data suggest that ACSS2 expression in enterocytes may reflect dietary fat intake to regulate the expression of genes involved in intestinal fat absorption and processing.

ACSS2 deletion perturbs lipid utilization during prolonged fasting

We next investigated the role of ACSS2 following prolonged fasting (48 h). Fasted ACSS2-/- mice were noticeably weaker and had reduced locomotor activity compared with

the ACSS2+/+ mice (data not shown). ACSS2-/- mice also lost significantly more body weight, which appeared due to increased loss of fat mass compared to lean mass (Figure 1.28). Epididymal fat mass levels were also significantly lower in ACSS2-/- mice following fasting (Figure 1.29).

I further analyzed several metabolic parameters in serum as a function of fasting. Glucose levels were significantly lower in ACSS2-/- mice compared with ACSS2+/+ mice after fasting (Figure 1.30). Consistent with the substantial reduction in adipose, non-esterified fatty acid concentrations were significantly higher in ACSS2-/- mice compared with ACSS2+/+ littermates, further suggesting a defect in the uptake of FA in ACSS2-/- mice. Serum ketone bodies (Figure 1.31) were reduced in ACSS2-/- mice after fasting, indicating that the mobilization and utilization of FA in ACSS2-/- livers might be perturbed. Consistent with these phenotypes, ACSS2-/- livers exhibited lowered expression of a panel of genes regulating FA transport and oxidation following fasting (Figure 1.32), while expression of FA transport genes were not significantly different on chow diet (Figure 1.33). On chow diet, there was no significant difference in resting glucose, serum NEFA, or ketone bodies between ACSS2+/+ and ACSS2-/- mice (Figure 1.23, 1.26).

I performed a global analysis of gene expression in ACSS2+/+ and ACSS2-/- mice livers after a 48 h fast. Pathway analysis revealed that the LXR/RXR pathway was significantly affected (Figure 1.34). LXR/RXR are transcription factors regulating lipid homeostasis in processes such as cholesterol metabolism, cholestrol biosynthesis, cholestrol transport, lipoprotein synthesis, lipogenesis, and cholesterol efflux. Multiple genes downstream of LXR/RXR controlling these processes were all down-regulated in ACSS2-/-

livers (Figure 1.35). These results suggest that the activity of ACSS2 impacts the expression and activation of LXR/RXR to affect fatty acid and sterol metabolism during prolonged fasting.

Discussion

In this study, we reveal that the acetyl-CoA synthetase enzyme ACSS2 regulates a coordinated, systemic response to impact lipid metabolism in the extremes of energy intake (high-fat feeding or prolonged fasting). During fasting, the exaggerated loss of adipose mass in ACSS2-/- mice indicates the capacity to hydrolyze TG in adipocytes. However, the concomitant accumulation of NEFA in blood (Figure 1.31) suggests inefficiency of FA clearance, uptake, and utilization, which is consistent with decreased expression of major FA transport genes such as CD36 and FABP1 in ACSS2-/- livers (Figure 1.32). A decrease in hepatic FA utilization by oxidation is further exemplified by the reduction in serum ketone body concentration, coincident with reduced expression of genes for mitochondrial FA oxidation (Figure 1.32). All of these observations suggest that the repartitioning of triglyceride energy from adipose tissue to the liver is perturbed in ACSS2-/- mice, strongly suggesting that a major function of this enzyme is to promote proper acquisition of energy from fat for organismal survival.

Under exposure to a high-fat diet, a consequence of this fat-dedicated function of ACSS2 is that it then promotes fat accumulation and hepatic steatosis. Loss of ACSS2 under HFD conditions leads to reduced expression of liver fatty acid transporters such as CD36 and FABP1 (Figure 1.15). Moreover, fatty acid transporters are also down-regulated in ACSS2-/-

enterocytes (Figure 1.23, 1.26), leading to less dietary lipid absorption (Figure 1.22) and more lipid in the feces (Figure 1.19), which further contribute to lowered serum lipid content (Figure 1.7). The correlation between nuclear expression of ACSS2 in enterocytes and the fed state (Figure 1.27) raises the possibility that the enzyme coordinates the expression of genes involved in fat absorption with dietary fat content. In response to a HFD, the enzyme would appear to promote optimal fat uptake and storage, leading to increased weight gain, fat stores, and hepatic steatosis.

The basic function of the ACS family of enzymes is to convert acetate and CoA into acetyl-CoA in an ATP-dependent reaction. We make note of a distinction between the role of mitochondrial versus nucleocytosolic ACS enzymes. Knockout mice lacking ACSS1 have been generated and show hypothermia and reduced energy production during fasted state (Sakakibara et al, 2009). These phenotypes are consistent with the idea that the retrieval of mitochondrial acetate mediated by ACSS1 contributes to mitochondrial energetics and thermogenesis especially upon starvation or cold shock. By contrast, the phenotypes reported here give evidence that ACSS2 may promote systemic fat utilization and storage through the selective, coordinated regulation of gene expression across multiple tissues. Our studies suggest that accumulation of nuclear acetate reflects the fasted state and fatty acid availability, and that acetate conversion to acetyl-CoA mediated by ACSS2 may represent an important signal that leads to the induction of genes in fat utilization, processing, and storage. As in vitro transcription from chromatin templates isolated from cells was significantly enhanced by histone acetylation (Nagai et al, 2017), the induction of these genes is likely dependent on the subsequent acetylation of histones mediated by local regeneration of

nuclear acetyl-CoA. As such, the nuclear presence of the ACSS2 enzyme enables the effects of a local acetate signal to be magnified and broadcast through epigenetic regulation of genes involved in lipid metabolism. We thus speculate that tumors which express ACSS2 may have enhanced capacity to utilize fats for cell growth or survival (Nieman et al, 2011; Blucher and Stadler, 2017).

Hepatic steatosis, which is the first and most reversible step in NAFLD, arises from an imbalance between hepatic TG acquisition and removal (Cohen et al, 2011). TGs are assembled by coupling three fatty acids to a glycerol backbone via ester bonds. The fatty acids that are responsible for hepatic TG formation primarily come from three sources: (i) diet, (ii) de novo synthesis, and (iii) adipose tissue (Cohen et al, 2011). In this study, we show how ACSS2 deficiency significantly affects all three sources.

We close by considering the perplexing value of the ACSS2 enzyme for both weight gain by animals availed an abundance of metabolic fuel, as well as survival under conditions of starvation. In the former case, it is sensible to consider the enzyme as a helpful conduit in building lipids for storage in adipose tissue and the liver. Less obvious, by contrast, is a logical consideration of how the ACSS2 enzyme might facilitate adaptation to starved conditions? In this regard we are reminded of histones as a depot for acetate storage (Comerford et al, 2014). Studies of yeast cells under fed or starved conditions have given evidence that the ACSS2 enzyme helps facilitate, under conditions of fuel abundance, acetylation of histone tails associated with genes involved in cell growth (Cai et al, 2011). Under conditions of starvation, the nuclear ACSS2 enzyme re-captures acetate resulting from histone de-acetylation and is required for re-distribution of this acetate to histone tails

associated with genes required for adaptation to starvation (Cai et al, 2011). Knowing that the half-life of histone-deposited acetate is measured in only minutes (Jackson et al, 1975; Waterborg, 2002), it can be understood that ACSS2 is responsible for the dynamic redistribution of acetate in a manner that directly regulates yeast cell adaptation to hydrocarbon fuel supply. The experiments give evidence that the nucleo-cytosolic ACSS2 enzyme of mammals may function via this same regulatory logic to adapt animals to either the fed or starved state. Given that ACSS2-null mice are viable, it is possible to imagine that a selective inhibitor of ACSS2 might represent a therapeutic strategy useful for the control of either fatty liver disease or obesity.

Summary

I investigated the role of acetate and ACSS2 in normal physiology and metabolism. By exposing mice to a high-fat diet or prolonged fasting, I found that ACSS2 promotes the proper storage or utilization of fat according to the fed or fasted state. The experiments give evidence that ACSS2 has an unanticipated function in the control of systemic lipid metabolism through selective modulation of gene expression linked to acetate availability.

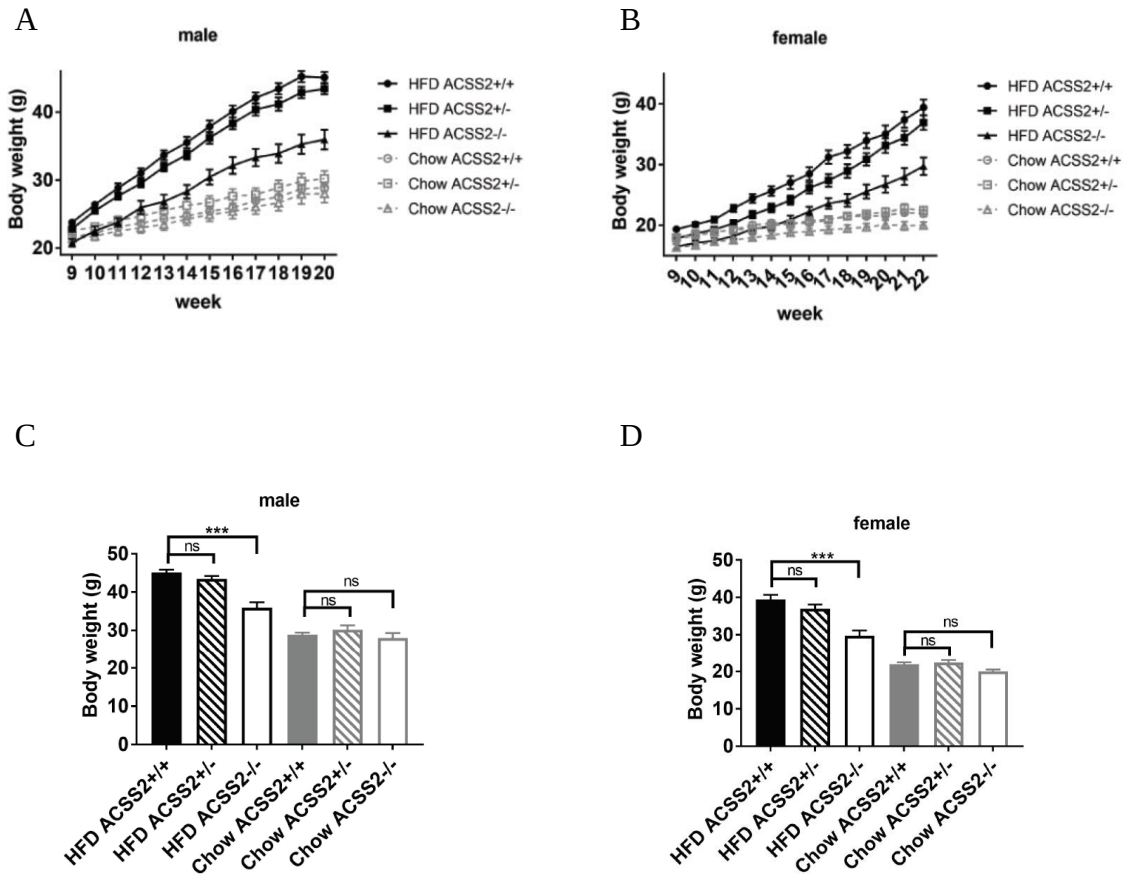

Figure 1.1 Body weights of ACSS2-/-, ACSS2+/- and ACSS2+/+ mice on HFD.
(A-B) Male (A) and female (B) ACSS2+/+, ACSS2+/-, and ACSS2-/- mice were fed chow or high-fat diet (HFD) starting at 9 weeks of age. Body weight was measured weekly (HFD: male ACSS2+/+ n=17, ACSS+/- n=24, ACSS2-/- n=14; female ACSS2+/+ n=15, ACSS2+/- n=20, ACSS2-/- n=11; chow diet: male ACSS2+/+ n=10, ACSS+/- n=11, ACSS2-/- n=8; female ACSS2+/+ n=9, ACSS2+/- n=13, ACSS2-/- n=9).
(C-D) Body weights of 20 week-old male (C) or 22 week-old female (D) ACSS2+/+, ACSS2+/-, and ACSS2-/- mice fed chow or HFD starting at 9 weeks as in A, B.

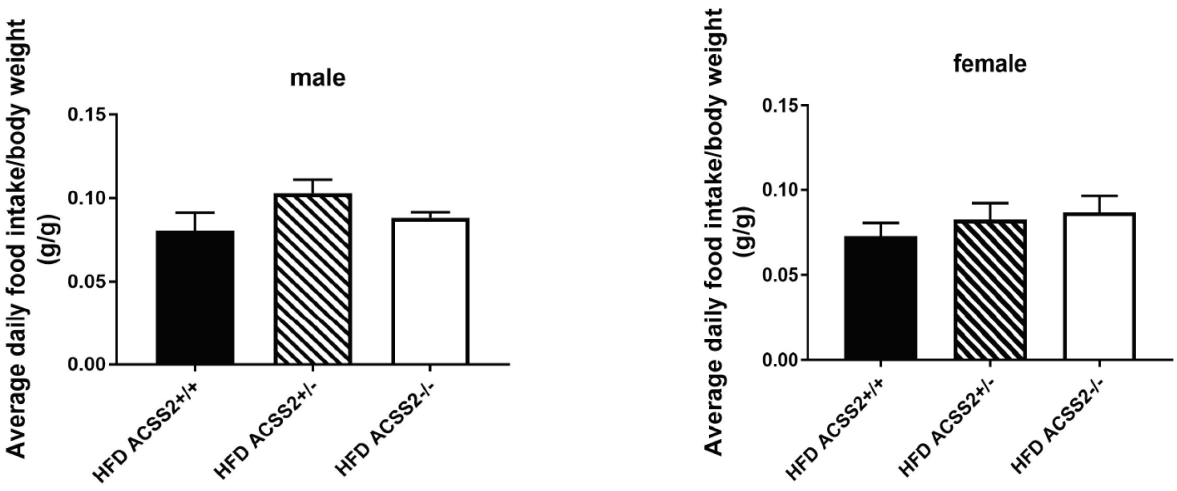

Figure 1.2 Food intake
Food intake was measured daily for ACSS2+/+, ACSS2+/-, and ACSS2-/- male (n=6) and female (n=7) mice on HFD. There was no significant difference between genotypes on HFD. Data reflect the mean ± SEM.

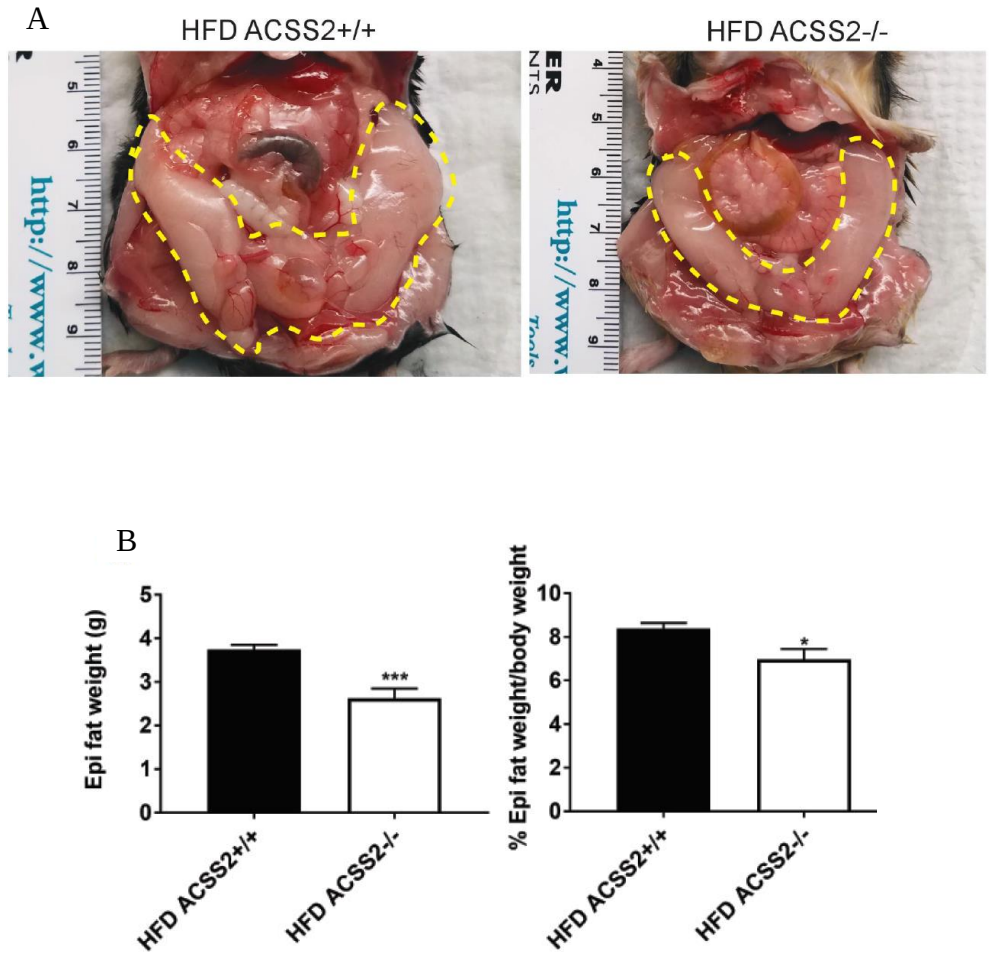

Figure 1.3 Epididymal fat mass was lower in ACSS2-/- mice.
(A) Representative images of epididymal fat pads of ACSS2+/+ and ACSS2-/- male mice fed a HFD for 12 weeks starting at 9 weeks of age.(B) Weight of epididymal fat depot was measured for ACSS2+/+ (n=14) and ACSS2-/- (n=11) male mice in HFD, and normalized to body weight. All data reflect the mean ± SEM, *p<0.05, **p<0.01, ***p<0.001.

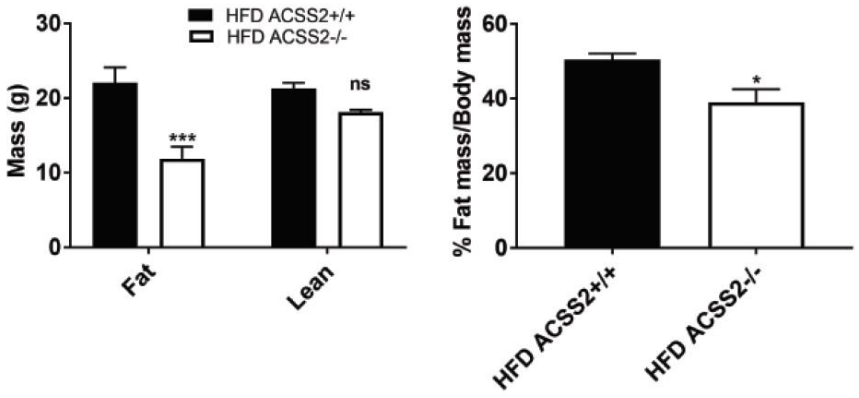

Figure 1.4 Body composition
Body composition as measured by NMR in ACSS2+/+ and ACSS2-/- male mice (n=5) fed a HFD, and normalized to body weight. All data reflect the mean ± SEM, *p<0.05, **p<0.01, ***p<0.001.

A

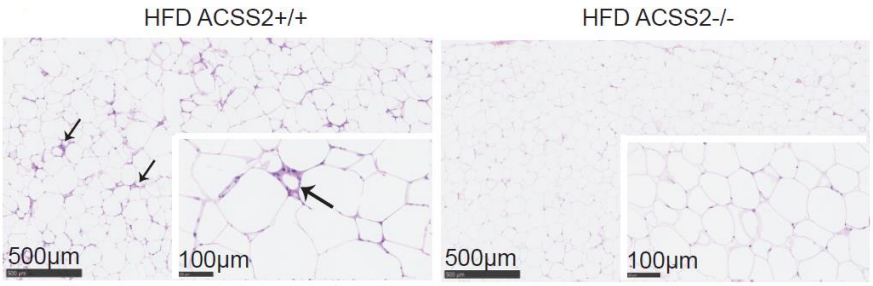

B

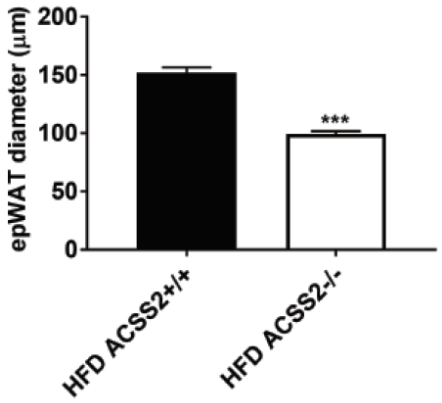

Figure 1.5 Adipocytes in ACSS2-/- mice showed a reduction in size.
(A) H&E staining of epWAT from male ACSS2+/+ and ACSS2-/- mice fed a HFD (n=3). Arrows denote inflammatory cells. Scale bars, 500 µm, and 100 µm. **(B)** Diameters of 60 epWAT cells from male ACSS2+/+ and ACSS2-/- mice fed a HFD (n=3). All data reflect the mean ± SEM, *p<0.05, **p<0.01, ***p<0.001.

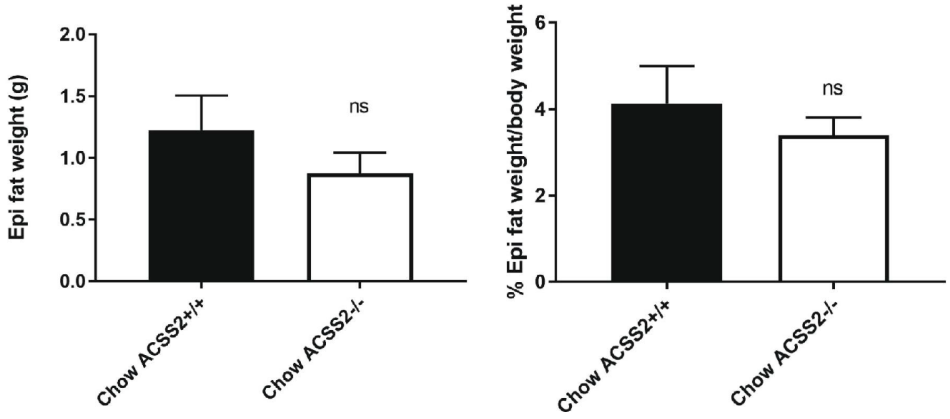

Figure 1.6 Weight of epi fat
Weight of epi fat was measured for ACSS2+/+ and ACSS2-/- male mice (n=5) fed in chow diet, and normalized to body weight. Data reflect the mean ± SEM. ns: non-significant.

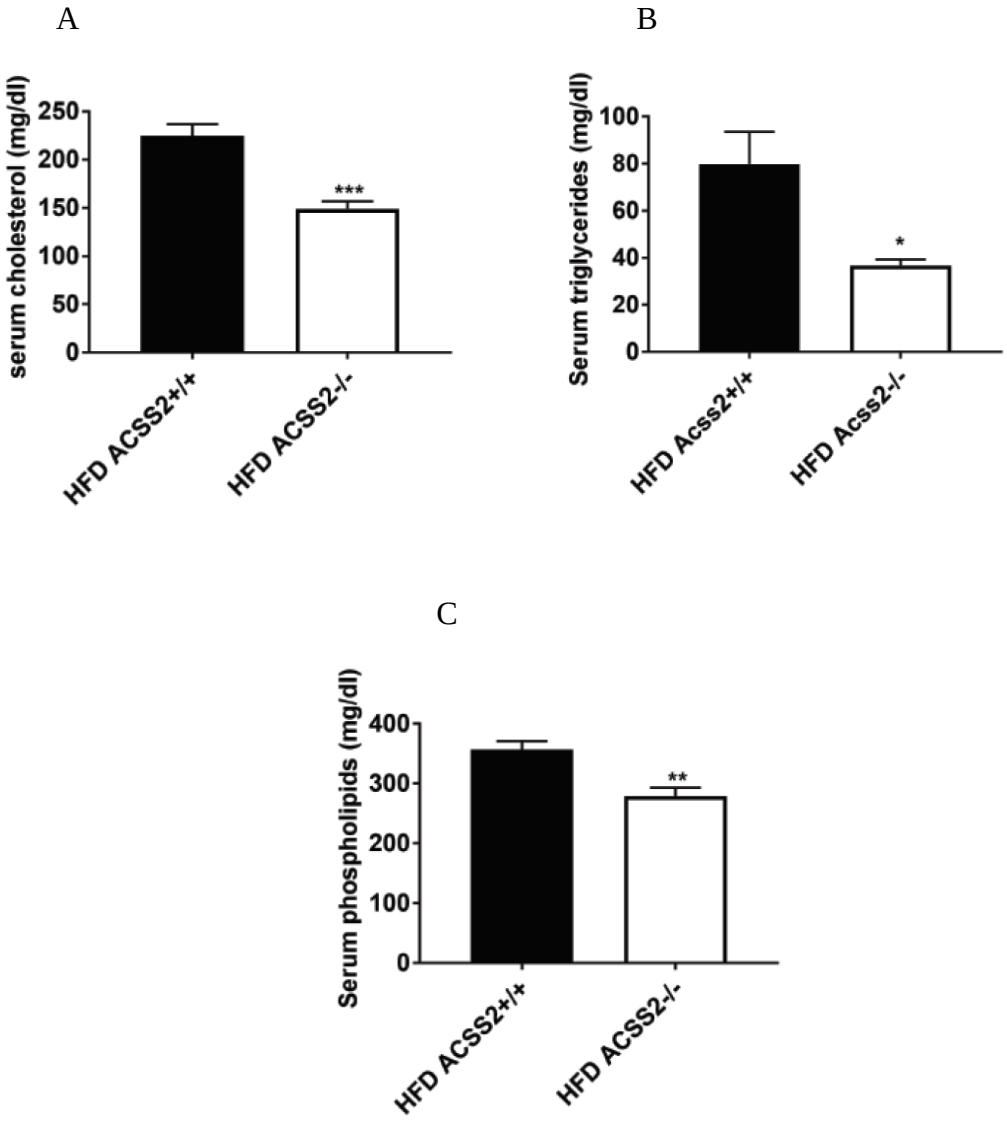

Figure 1.7 Serum cholesterol, triglyceride, and phospholipid concentrations under HFD. Serum cholesterol (A) (n=10), triglycerides (B) (n=7), and phospholipids (C) (n=10) in ACSS2+/+ and ACSS2-/- male mice fed a HFD. All data reflect the mean ± SEM, *p<0.05, **p<0.01, ***p<0.001.

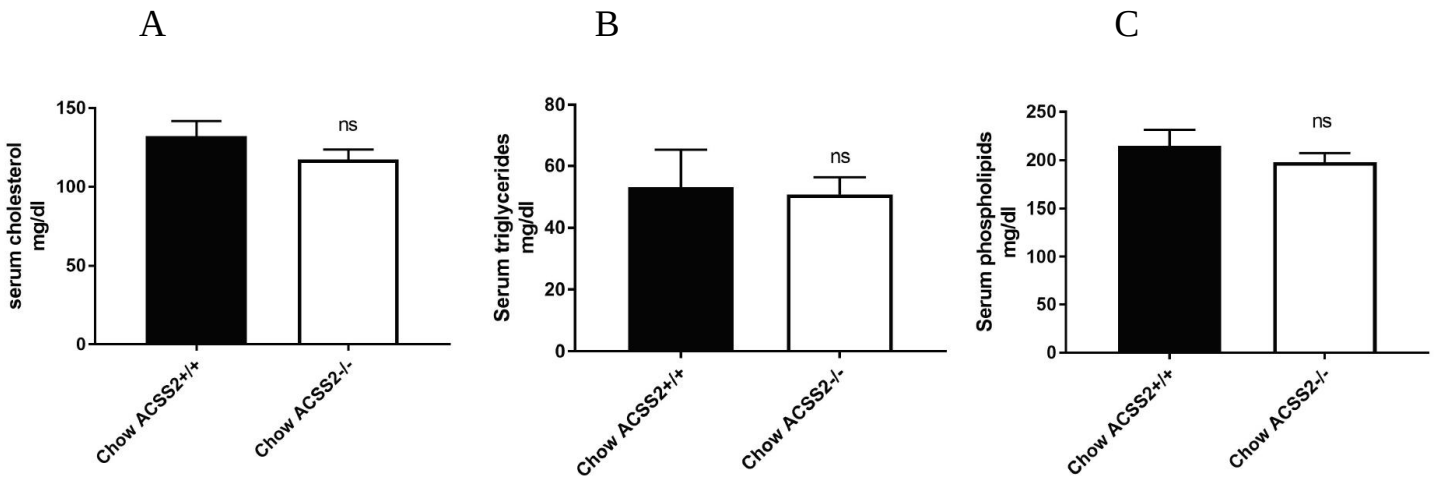

Figure 1. Serum cholesterol, triglyceride, and phospholipid concentrations under chow diet.

Serum cholesterol (A), triglycerides (B), and phospholipids (C) concentration in ACSS2+/+ and ACSS2-/- male mice (n=5) on chow diet. Data reflect the mean ± SEM. ns: nonsignificant.

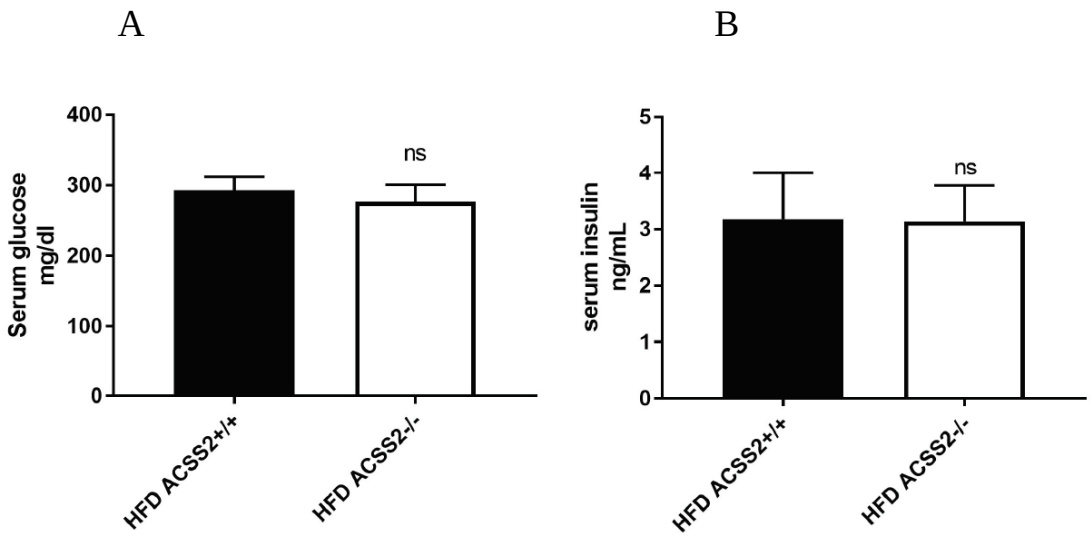

Figure 1.9 Serum glucose and insulin.
Serum glucose (A) (n=12) and insulin (B) (n=5) concentration in ACSS2+/+ and ACSS2-/- male mice fed a HFD for 12 weeks starting at 9 weeks of age. Data reflect the mean ± SEM. ns: non-significant.

A

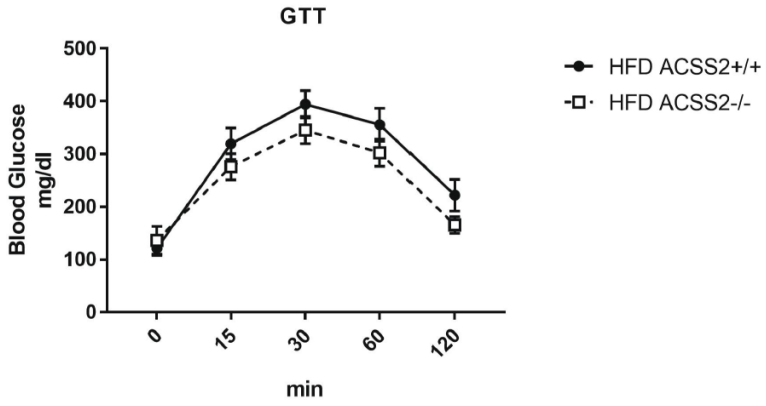

B

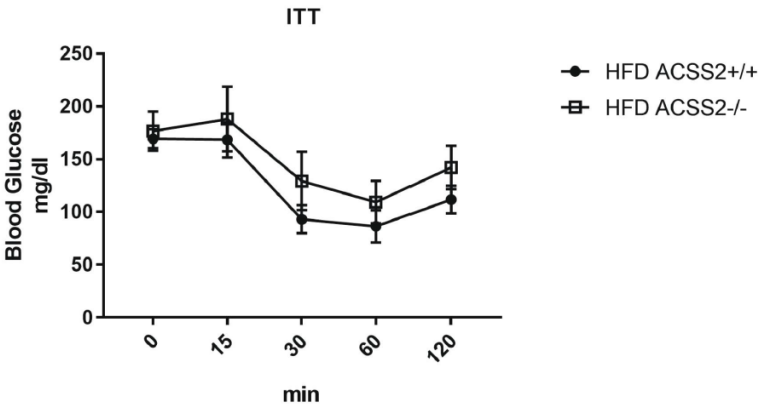

Figure 1.10 GTT and ITT.
(A) Blood glucose during glucose tolerance test (GTT) in overnight-fasted ACSS2+/+ (n=16) and ACSS2-/- (n=14) male mice fed a HFD for 12 weeks. (B) Blood glucose during insulin tolerance test (ITT) in 4 h-fasted ACSS2+/+ (n=12) and ACSS2-/- (n=9) male mice fed a HFD for 12 weeks. Data reflect the mean ± SEM.

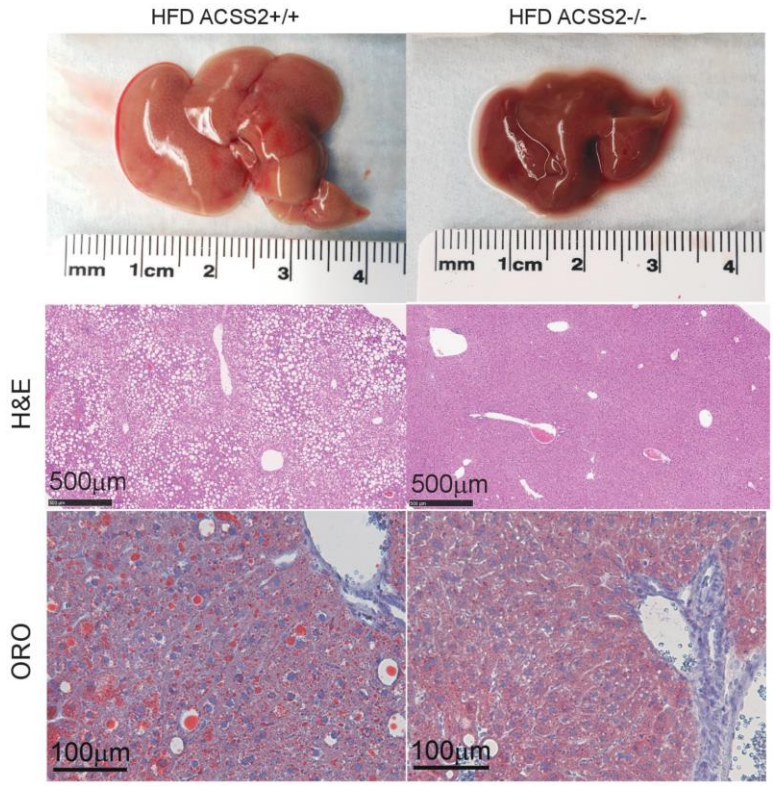

Figure 1.11 Hepatic steatosis in mice fed a HFD.
General liver appearance**,** Haematoxylin and eosin (H&E) and oil red O (ORO) imaging from representative male mice fed a HFD for 12 weeks starting at 9 weeks of age. Scale bar, 500 µm.

A

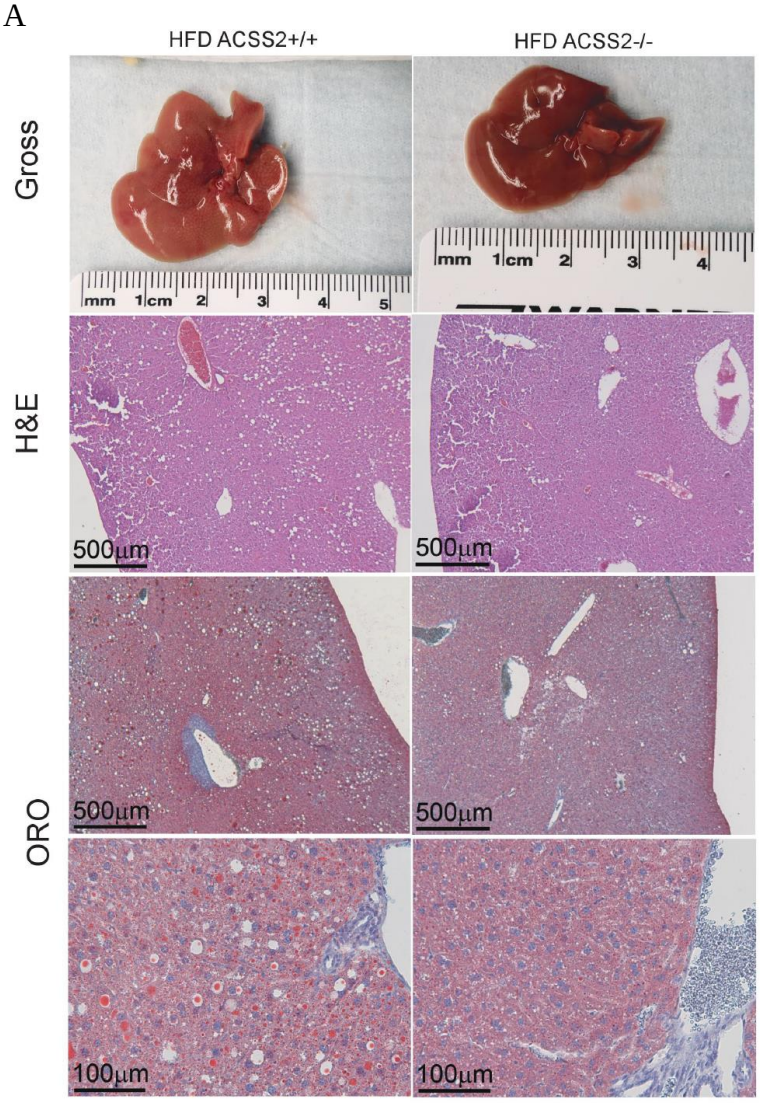
HFD ACSS2+/+
HFD ACSS2-/-
Gross
H&E
ORO
500μm
100μm

B

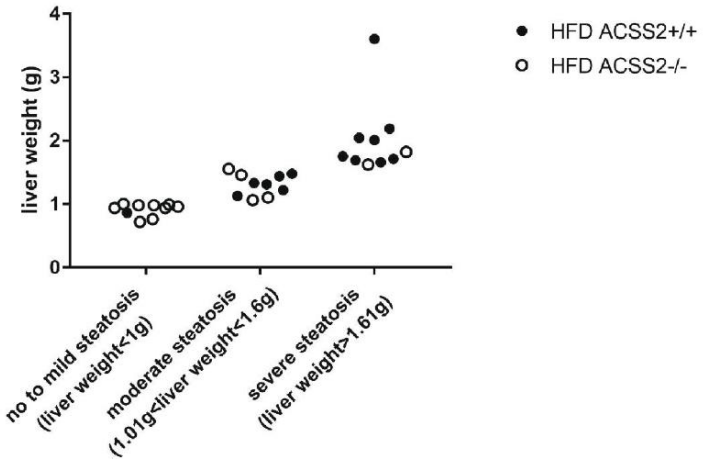
liver weight (g)
0
1
2
3
4
HFD ACSS2+/+
HFD ACSS2-/-
no to mild steatosis (liver weight<1g)
moderate steatosis (1.01g<liver weight<1.6g)
severe steatosis (liver weight>1.61g)

Figure 1.12 Hepatic steatosis in mice fed a HFD.
(A) Gross, Haematoxylin and eosin (H&E), and oil red O images of livers from additional representative male mice fed a HFD for 12 weeks. Scale bars, 500 μm and 100 μm. (B) Distribution of hepatic steatosis. ACSS2+/+ and ACSS2-/- male mice (n=15) fed a HFD for 12 weeks starting at 9 weeks of age were categorized into no to mild steatosis (liver weight<1g), moderate steatosis (1.01g<liver weight<1.6g), and severe steatosis (liver weight>1.61g).

A

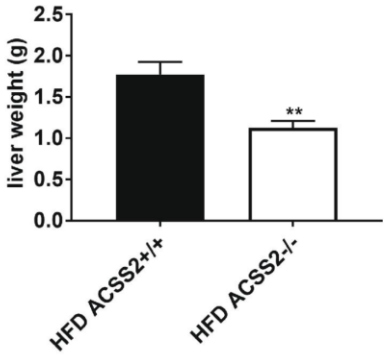

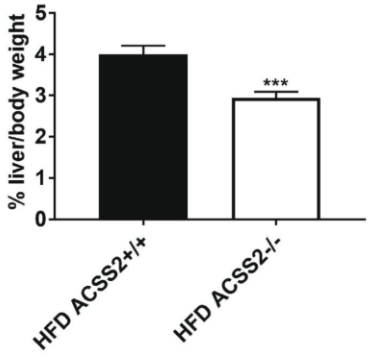

B

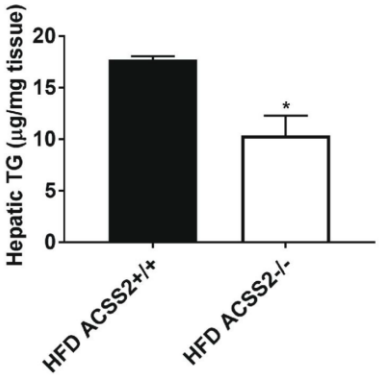

Figure 1.13 Liver mass and liver triglyceride.
(A) Mass of livers from ACSS2+/+ and ACSS2-/- male mice fed a HFD for 12 weeks (n=15), and normalized to body weight. Data represent mean ± SEM. **p<0.005. (B) Hepatic TG of male mice fed a HFD for 12 weeks (n = 5). Data represent mean ± SEM. *p<0.05.

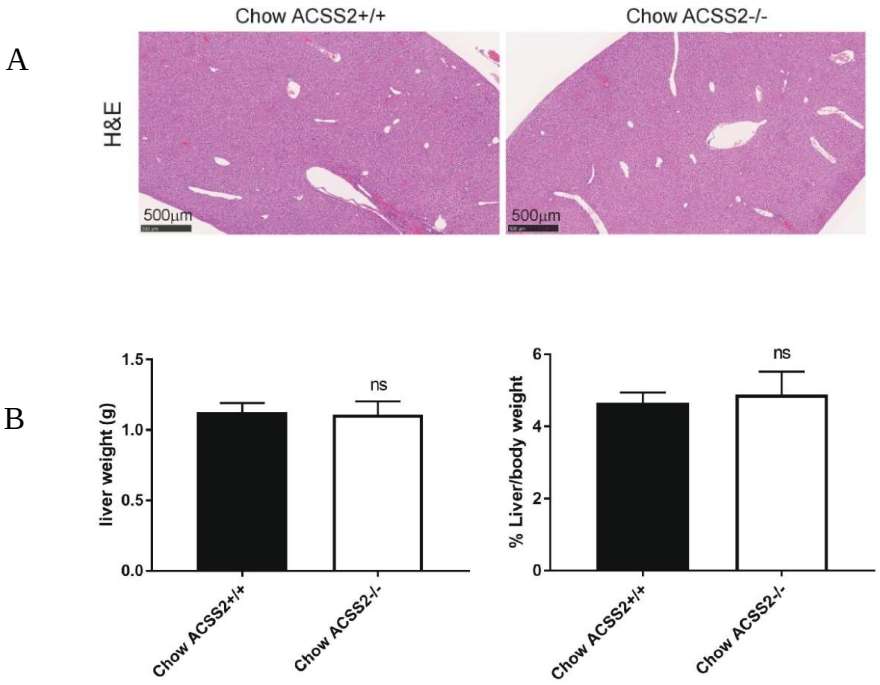

Figure 1.14 Under chow diet conditions, ACSS2-/- livers were comparable to WT livers. (A) Haematoxylin and eosin (H&E) images of livers from additional representative male mice on chow diet. Scale bar, 500 µm. (B) Liver weights were measured for ACSS2+/+ and ACSS2-/- male mice (n=5) fed a chow diet, and normalized to body weight.

A

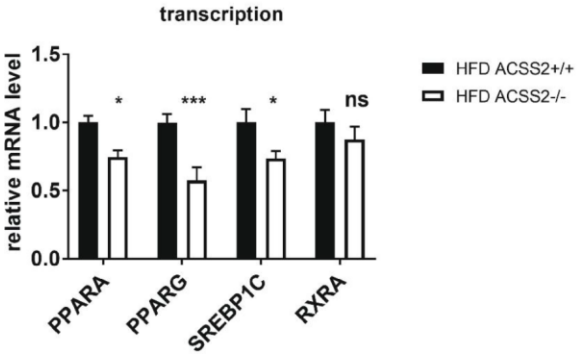

B

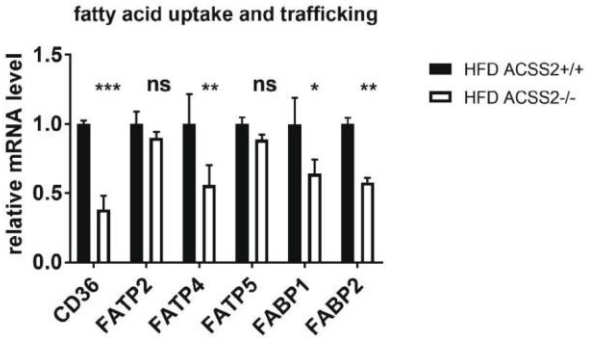

Figure 1.15 The expression of transcriptional regulators of lipid metabolism and key genes involved in fatty acid uptake and trafficking.
Hepatic mRNA levels of male mice fed a HFD for 12 weeks (n = 4). Data reflect the mean ± SEM. ns: not significant, *p<0.05, **p<0.01.

A

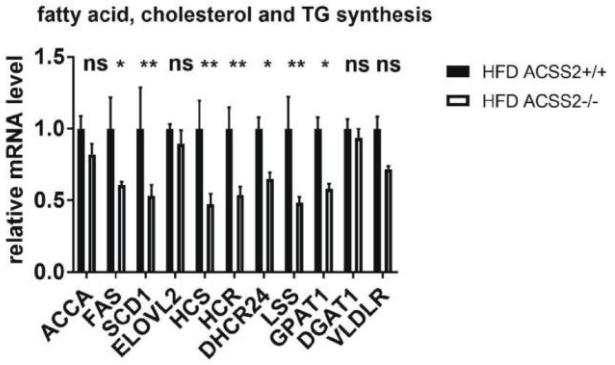

B

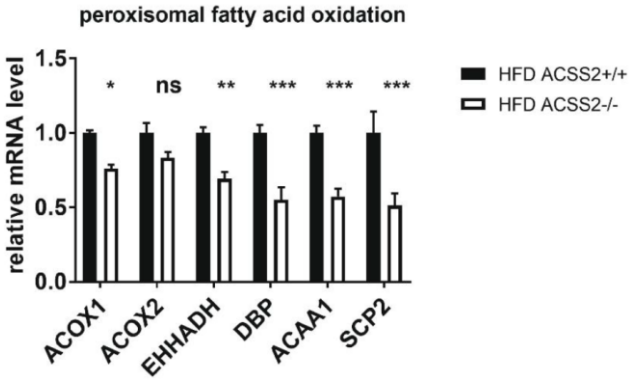

Figure 1.16 The expression of key genes involved in lipid synthesis and peroxisomal fatty acid oxidation.

Hepatic mRNA levels of male mice fed a HFD for 12 weeks (n = 4). Data reflect the mean ± SEM. ns: not significant, *p<0.05, **p<0.01.

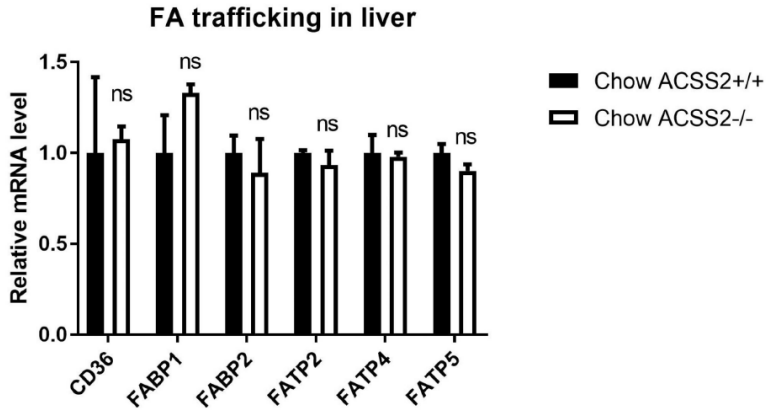

Figure 1.17 The expression of genes involved in fatty acid uptake and transport on chow diet.

mRNA expression of FA transporters in liver of male mice on chow diet (n=3). All data reflect the mean ± SEM. ns: not significant.

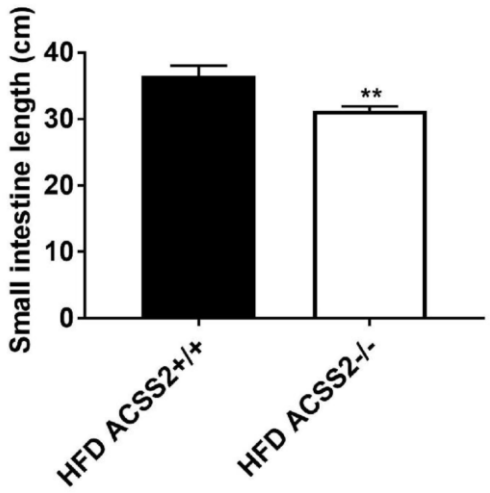

Figure 1.18 The length of the small intestine.
The average length of small intestine of ACSS2+/+ and ACSS2-/- male mice fed a HFD for 12 weeks starting at 9 weeks of age (n=15). Data represent mean ± SEM. **p<0.01.

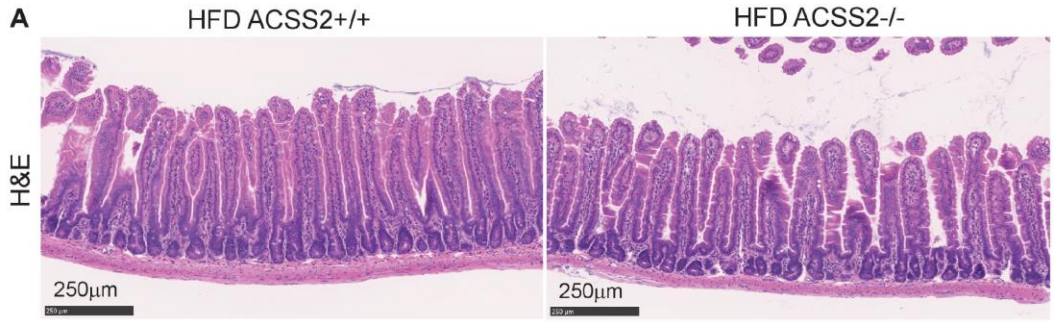

Figure 1.19 ACSS2-/- mice exhibit slightly shorter villi
Haematoxylin and eosin (H&E) images of proximal intestinal samples from ACSS2+/+ and ACSS2-/- male mice fed a HFD for 12 weeks starting at 9 weeks of age. Scale bar, 250 µm.

A

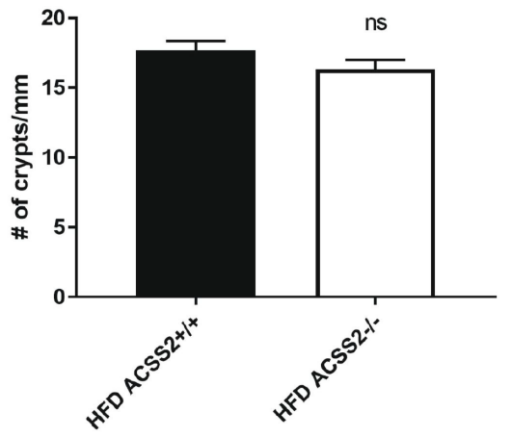

B

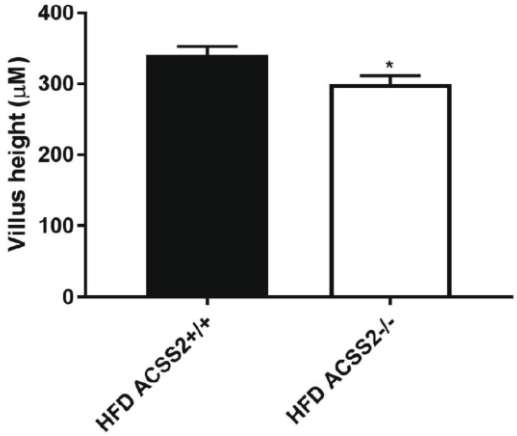

Figure 1.20 ACSS2-/- mice exhibit slightly shorter villi
Crypt numbers (A) and villus height (B) of ACSS2+/+ and ACSS2-/- male mice fed a HFD for 12 weeks (n=3).

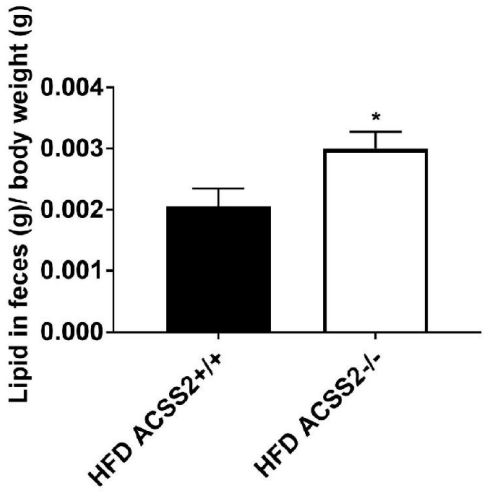

Figure 1.21 Fecal lipid content in mice fed a HFD
Fecal lipid content was analyzed from male mice fed a HFD for 12 weeks (n=6). *$p<0.05$, ns: non-significant.

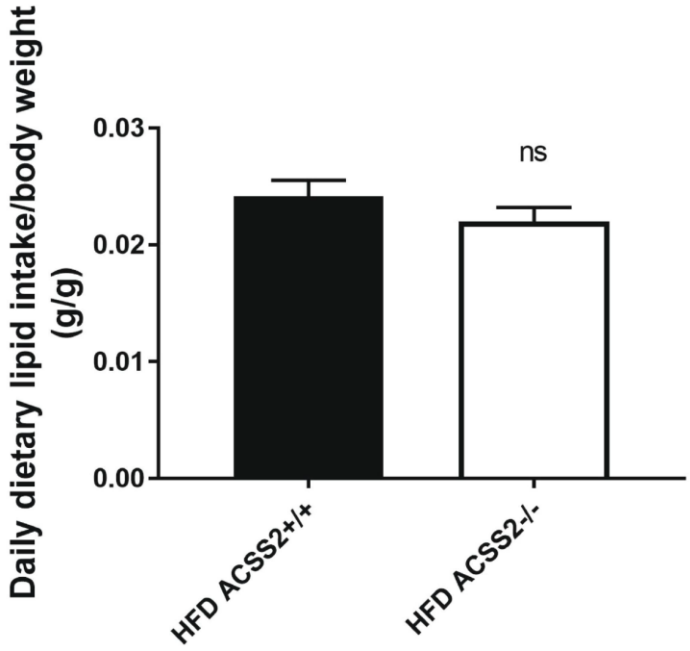

Figure 2.22 Daily dietary lipid intake
Daily dietary lipid intake was analyzed in male mice fed a HFD for 12 weeks (n=6), ns: non-significant.

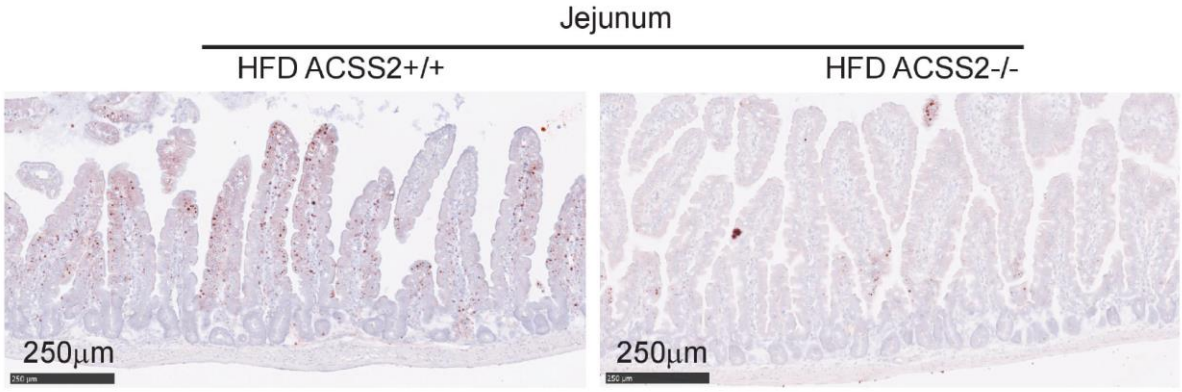

Figure 1.23 ORO staining of proximal intestines
ORO staining of proximal intestines from a representative male mouse of the indicated genotype fed a HFD for 12 weeks. Scale bar, 250 μm. On HFD, fewer and smaller lipid droplets were observed in the mucosa of the proximal intestine of ACSS2-/- mice.

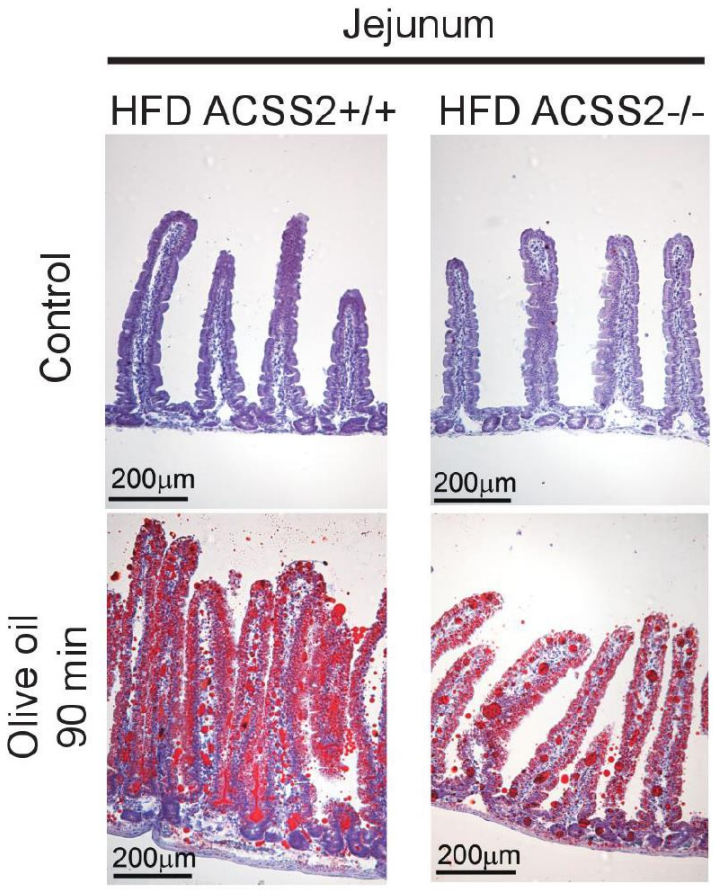

Figure 1.24 ORO staining of proximal intestine with or without olive oil gavage
ORO staining of proximal intestines from representative male mice fed a HFD for 12 weeks with or without olive oil by oral gavage after overnight fasting. Scale bar, 200 μm. Fewer and smaller lipid droplets were noted in the mucosa of the proximal intestine of ACSS2-/- mice after olive oil gavage.

A

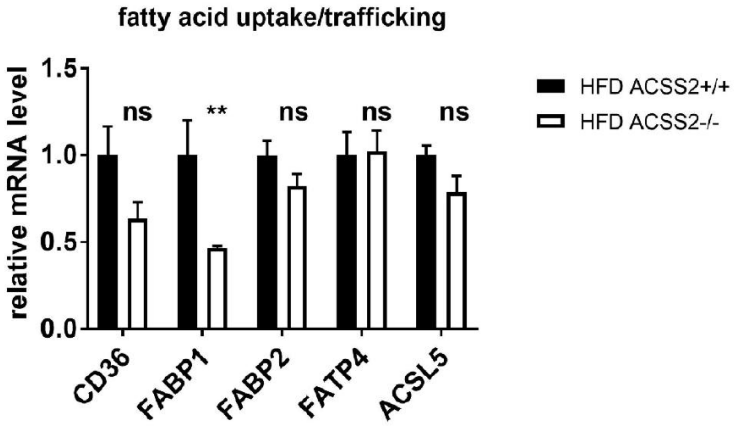

B

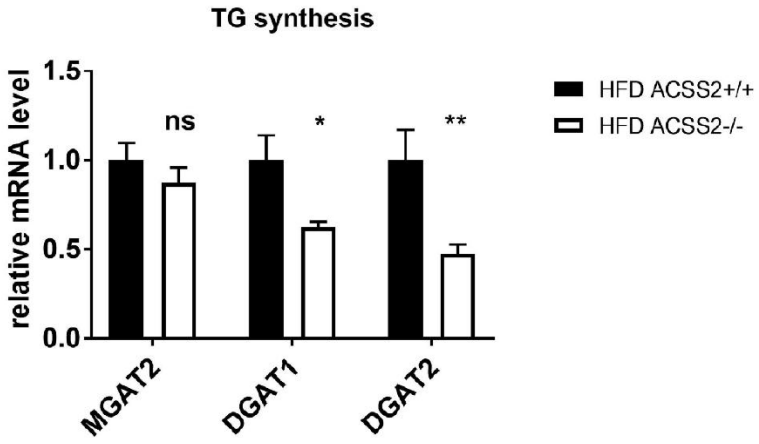

Figure 1.25 The expression of key genes involved in fatty acid transport and TG synthesis.

Intestinal mRNA profile of male mice fed a HFD for 12 weeks (n=4). Data reflect mean ± SEM. ns: nonsignificant, *p<0.05, **p<0.01.

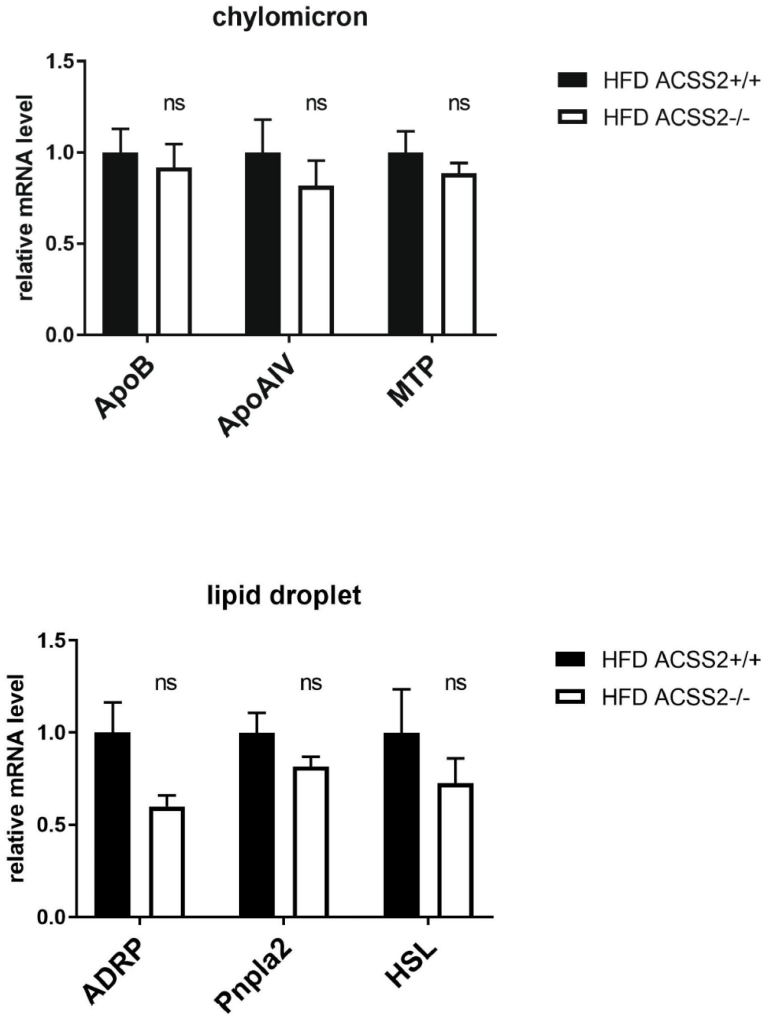

Figure 1.26 The expression of genes involved in droplet dynamics and chylomicron assembly and secretion.
Intestinal mRNA profile of male mice fed a HFD for 12 weeks (n=4). Data reflect the mean ± SEM. ns: not significant.

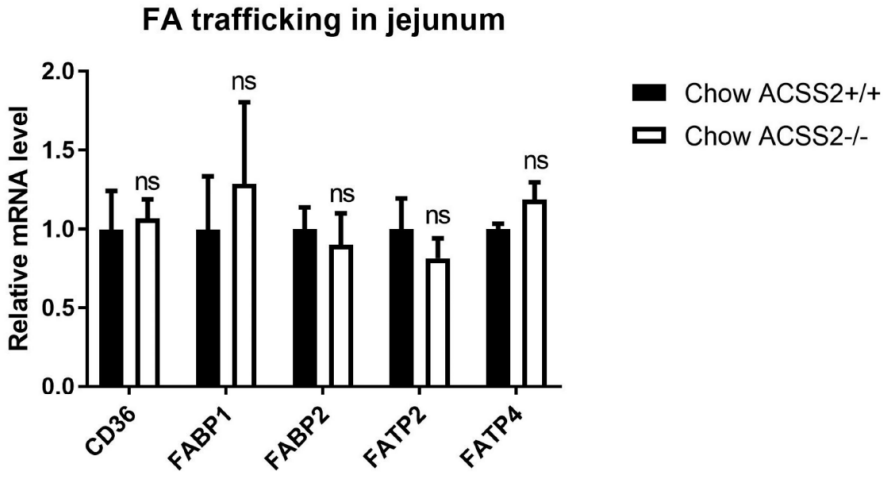

Figure 1.27 Intestinal mRNA profile of male mice on chow diet
Intestinal mRNA profile of male mice on chow diet (n=3). Data reflect the mean ± SEM. ns: not significant. On chow diet, no difference was observed in expression of genes involved in dietary lipid uptake between WT and KO small intestine.

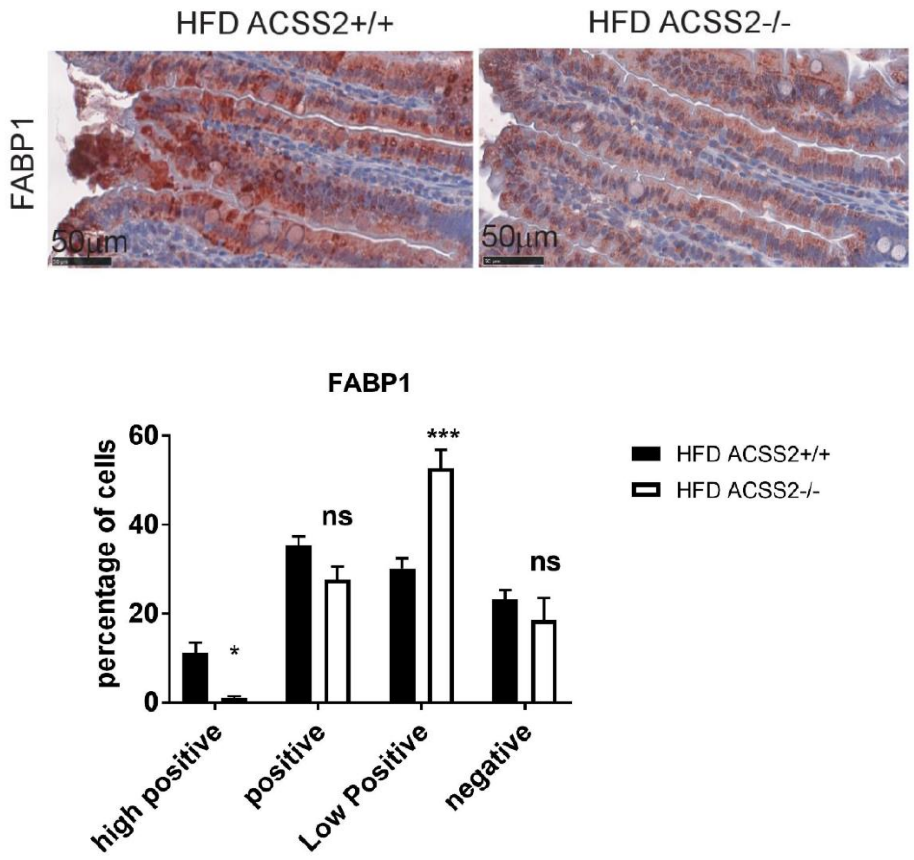

Figure 1.28 FABP1 protein level in enterocytes
FABP1 immunohistochemical staining of proximal small intestine from ACSS2+/+ and ACSS2-/- male mice fed a HFD for 12 weeks. Scale bar, 50 µm. Quantitative evaluation and automated scoring of FABP1 expression was analyzed by IHC Profiler22. FABP1 protein level reduced in the enterocytes of ACSS2-/- mice.

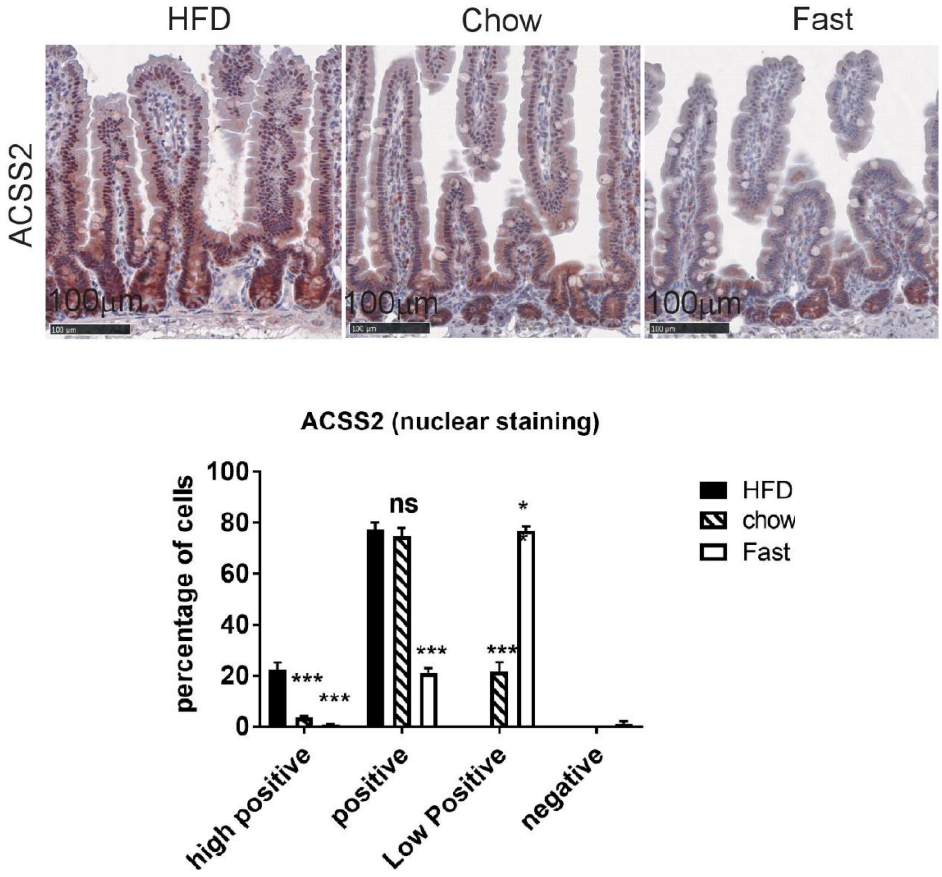

Figure 1.29 The distribution of ACSS2 protein in intestinal enterocytes and in cells of the intestinal crypt

IHC staining of ACSS2 protein expression in proximal intestines from male mice fed either HFD for 12 weeks, chow diet, or fasted for 48 h. Scale bar, 100 µm. Quantitative evaluation and automated scoring of nuclear ACSS2 expression was performed by IHC Profiler22.

A

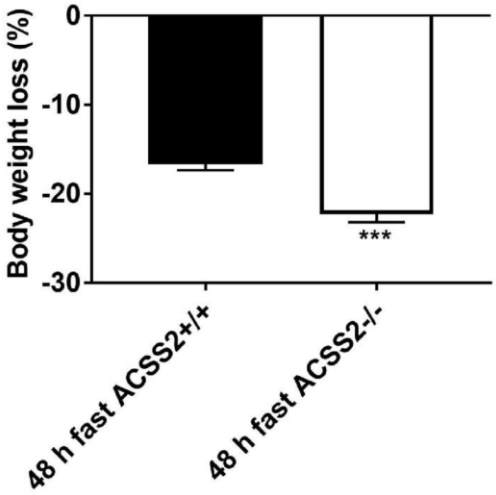

B

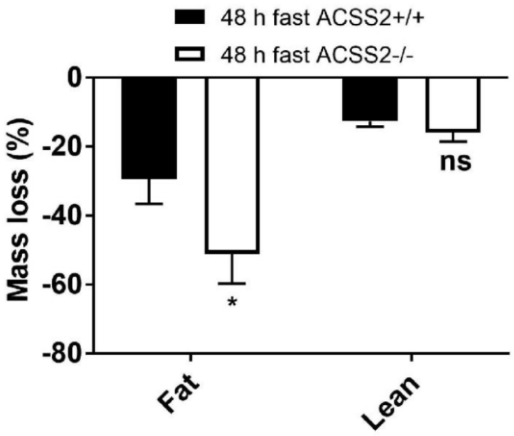

Figure 1.30 Body weight loss and fat mass loss during prolonged fasting
(A) Percentage reduction in body weight of ACSS2+/+ (n=10) and ACSS2-/- (n=8) male mice after 48 h fast. Mice were on chow diet prior to fasting. (B) Percent reduction in fat and lean mass in ACSS2+/+ and ACSS2-/- male mice (n=3) after 48 h fast. During prolonged fasting, ACSS2-/- mice lost significantly more body weight, which appeared due to increased loss of fat mass compared to lean mass.

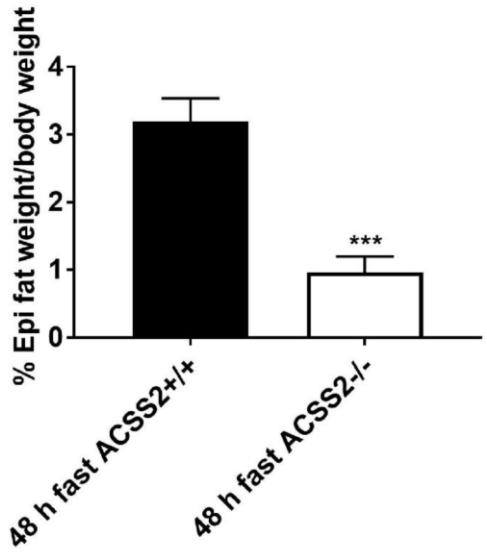

Figure 1.31 Epididymal fat mass in ACSS2+/+ and ACSS2-/- mice following fasting
Weight of epididymal fat depot was measured for ACSS2+/+ (n=10) and ACSS2-/- (n=8) male mice after a 48 h fast, and normalized to body weight. Epididymal fat mass was lower in ACSS2-/- mice following fasting.

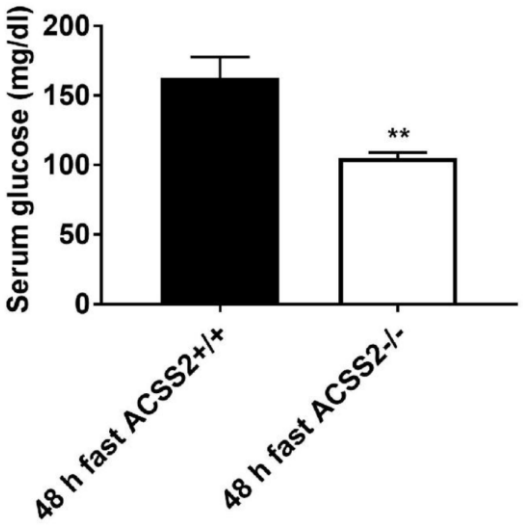

Figure 1.32 Glucose level mice after fasting
Serum glucose concentration in ACSS2+/+ (n=10) and ACSS2-/- (n=8) male mice after 48 h fast. Glucose level was lower in ACSS2-/- mice compared to WT after fasting.

A

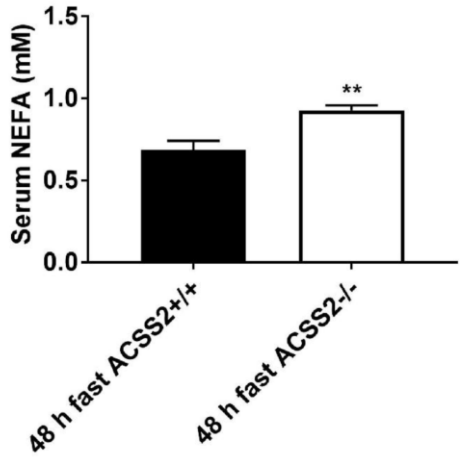

B

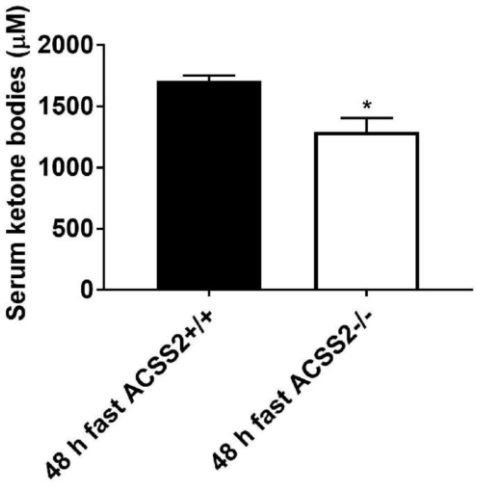

Figure 1.33 Non-esterified fatty acid and serum ketone bodies concentrations.
(A) Nonesterified fatty acid concentration in ACSS2+/+ (n=10) and ACSS2-/- (n=8) male mice after 48 h fast. (B) Serum ketone bodies concentration in ACSS2+/+ (n=10) and ACSS2-/- (n=8) male mice after 48 h fast.

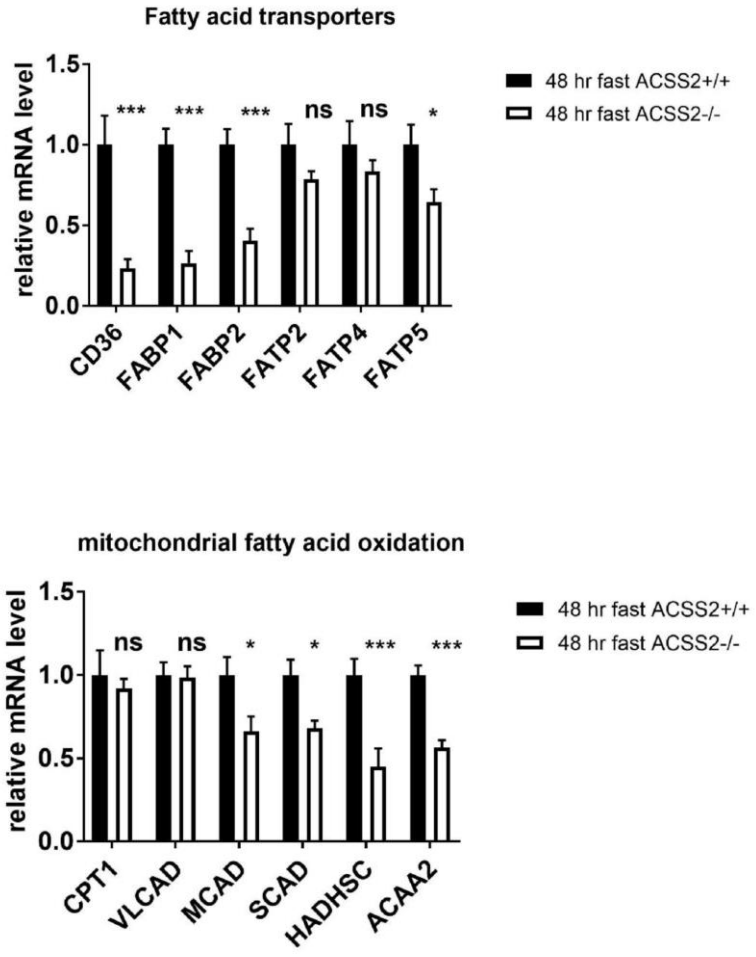

Figure 1.34 The expression of genes regulating fatty acid transport and oxidation following fasting

Hepatic mRNA profile of ACSS2+/+ and ACSS2-/- male mice after 48 h fast (n=5). All data reflect the mean 8 ± SEM. ns: not significant, *p<0.05, **p<0.01.

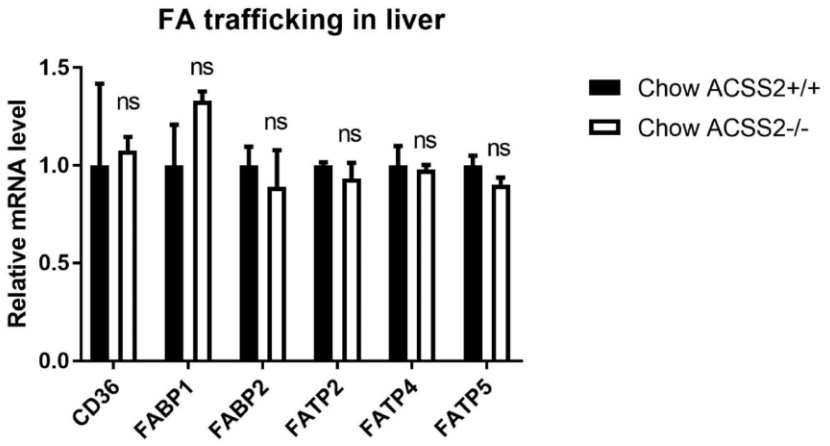

Figure 1.35 The expression of fatty acid transport genes in mice on chow diet
mRNA expression of FA transporters in liver of male mice on chow diet (n=3). All data reflect the mean ± SEM. ns: not significant.

A

Top Canonical Pathways

Name	p-value	Overlap
LPS/IL-1 Mediated Inhibition of RXR Function	3.07E-10	29% (64/221)
Superpathway of Cholesterol Biosynthesis	4.40E-08	57.1% (16/28)
LXR/RXR Activation	3.66E-07	30.6% (37/121)
NF-κB Signaling	2.10E-06	26% (47/181)
Hepatic Fibrosis/Hepatic Stellate Cell Activation	2.99E-06	25.7% (47/183)

B

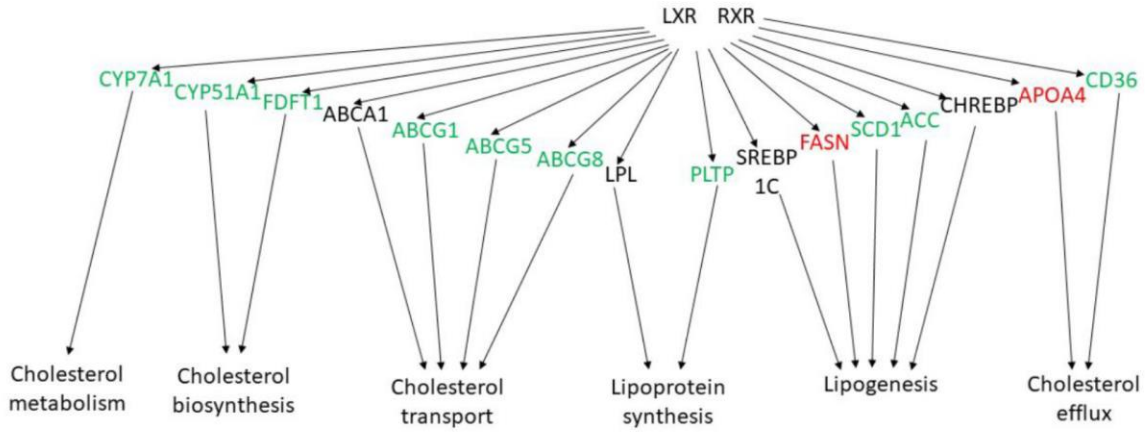

Figure 1.36 Global analysis of gene expression in ACSS2+/+ and ACSS2-/- liver after 48 h fast.

(A) RNA-seq was performed with hepatic mRNA from ACSS2+/+ and ACSS2-/- male mice after 48 h fast (n=3). Top affected pathways are indicated. (B) Genes with increased expression (red), decreased expression (green), and no change (black) in ACSS2-/- livers are indicated, and segregated by function using IPA pathway analysis.

CHAPTER TWO

Critical Role of Acetyl-CoA Synthetase 2 in the Development of Pancreatic Cancer

Introduction

Acetate is a metabolite present in the human blood at concentrations ranging from 50 to 200 μM (Tollinger et al, 1979). Intracellular acetate can also be produced from deacetylation reactions such as histone deacetylation, which is a very dynamic and robust process. Cytosolic acetate can be converted into acetyl-CoA, which is an important intermediary metabolite for lipid synthesis as well as an acetyl group donor for acetylation modification of proteins such as histones. The conversion of cytosolic acetate into acetyl-CoA is catalyzed by acetyl-CoA synthetases 2 (ACSS2). Our laboratory previously has observed that loss of ACSS2 reduced tumor burden in two models of hepatocellular carcinoma in mice (Comerford et al, 2014), suggesting that the development of hepatocellular carcinoma can be dependent on acetate. This acetate dependence in hepatocellular carcinoma could be common to other types of cancer as ^{11}C acetate PET has been successfully applied clinically to detect various types of cancers, including pancreatic ductal adenocarcinoma (PDAC) (Zhao et al, 2009; Shreve and Gross, 1997). We have demonstrated that ACSS2 expression in PDAC mouse model KIC (Aguirre et al, 2003) showed that ACSS2 was absent in normal pancreatic tissue but expressed at very high levels in precancerous lesions of PDAC. I found that absence of ACSS2 in the KIC model reduced

the tumor burdens, and ACSS2 expression is correlated with tumor size (stage?). These data indicate that ACSS2 has a potential function in the development of PDAC.

PDAC is the 4th leading cause of cancer related deaths in the United States with a five-year survival rate of only 6%. The poor prognosis of PDAC can be attributed to the fact that the disease is often diagnosed at a late stage. Development of an early detection strategy and an effective therapeutic intervention is crucial to the treatment of PDAC (Urayama, 2015). IHC staining results showed that expression of ACSS2 is induced in the early phase of PDAC development, namely pancreatic intraepithelial neoplasia (PanIN) I and II lesions, indicating that ACSS2 may be important in the early phase of PDAC development. Several clinical studies with ^{11}C acetate PET imaging suggested *in vivo* utilization of acetate in PDAC patients (Zhao et al, 2009; Shreve and Gross, 1997). Our previous study showed that [^{11}C] acetate uptake correlated with ACSS2 expression in liver cancer (Comerford et al, 2014). The evidence indicates that acetate uptake may be a potential marker for early detection of PDAC.

ACSS2 expression in mouse pancreatic cancer

ACSS2 expressed in most of the organs in the GI tract of the mouse including liver, kidneys, WAT and intestine (Luong et al, 2000). We examined ACSS2 expression in pancreas. ACSS2 did not express in mouse pancreas from E12.5 to adult. In contrast, ACSS2 expression appeared in liver starting from E14.5 (Figure 2.1). These results indicated that ACSS2 is not involved in the normal function of pancreas in mice. However, we found an elevation of ACSS2 expression in the pancreas during tumorigenesis in the KIC (Figure 2.2)

as well as KPC (Figure 2.3) models of PDAC. Interestingly, we found ACSS2 exhibited the most expression in the low-grade and moderate grade lesions, for instance the PanIN-1A, PanIN-1B, and PanIN-2, which have the minimal to moderate cytological and architectural atypia (Distler et al, 2014). However, the expression of ACSS2 decreased in the high-grade PanIN (PanIN-3) which have severe cytological and architectural atypia (Figure 2.4).

PanINs are developed from exocrine component of pancreas which comprises acinar cells, and ductal cells. However, the cell of origin for PanINs in KRAS-activated genetically engineered mouse PDAC models is still not clear (Oldfield et al, 2017). We analyzed expression of ACSS2, duct cell marker SOX9, and acinar cell marker Amylase in serial KIC sections and found that ACSS2 expression was associated with SOX9 but not Amylase (Figure 2.5), indicating that ACSS2 is associated with the PanINs originated from ductal cells.

Besides PanINs, PDAC can also develop from intraductal papillary mucinous neoplasms (IPMN), which is derived from pancreatic cysts. ACSS2 was expressed in the IPMN mouse PDAC model $Kras^{G12D}$, $Arid1a^{-/-}$, p48Cre (KAC) but not the normal pancreas (Figure 2.6) suggesting ACSS2 activation is preserved in different types of distinct intermediary precursor lesions of PDACs.

ACSS2 expression in human pancreatic cancer

ACSS2 was not expressed in adult human normal pancreas tissues, indicating ACSS2 function is not essential in normal human pancreas. Interestingly, ACSS2 expression was elevated in both PanIN and IPMN in human PDAC (Figure 2.7). A tissue microarray (TMA)

was constructed from 64 surgically excised human pancreatic ductal adenocarcinomas. Immunohistochemical staining of ACSS2 was performed on this array which was read by an experienced pathologist. We found that ACSS2 expression is correlated with tumor grade. ACSS2 is highly expressed in tumor grade 1 and 2 but its expression level is reduced in grade 3 and 4 (Figure 2.8).

ACSS2 deficiency suppress PDAC development in KIC

To evaluate the contribution of ACSS2 to PDAC development and progression, we used KIC (LSL-$Kras^{G12D/+}$; $Cdkn2a^{Lox/Lox}$; $p48^{Cre}$; (Aguirre et al, 2003)) mice, which is a well-established genetically engineered mouse model (GEMM) of PDAC. KIC animals express a constitutively active form of Kras and have biallelic inactivation of the Cdkn2a locus. The tumorigenesis in pancreas was driven by $p48^{Cre}$ (also known as Ptf1a), which is expressed in pancreatic bud progenitor cells (Kawaguchi et al, 2002). ACSS2-/- mice are viable, fertile and phenotypically normal compared with ACSS2+/+ mice (Comerford et al, 2014). To study the contribution of ACSS2 to PDAC development, we crossed ACSS2+/- mice with KIC animals to generate genetically matched ACSS2+/+KIC, ACSS2+/-KIC, and ACSS2-/-KIC mice. The pancreas/body weight was significantly smaller in ACSS2-/-KIC than ACSS2+/+KIC mice at 8 weeks (Figure 2.9). The pancreas/body weight in ACSS2+/-KIC mice had a big variation but was still significantly different from ACSS2+/+KIC mice, suggesting that losing one copy of ACSS2 may have tumor suppressive effect (Figure 2.9). The pancreas weight (Figure 2.10) and size (Figure 2.11) of animals in different genotypes correlated with the trends in pancreas/body weight. At 8 weeks, the ACSS2+/+KIC

pancreases were abounded with PanINs and PDAC, while in ACSS2-/-KIC pancreases, the pancreases were still relatively normal and abounded with normal acinar cells while PanIN-1 emerged in a few regions (Figure 2.12). The variation in pancreas weight in 8 weeks old ACSS2+/-KIC mice led us to examine the ACSS2 expression in these individual pancreases. ACSS2+/-KIC mice were divided into three groups according to their pancreas weight: mild (pancreas weight<0.4 g), medium (0.4 g<pancreas weight<0.8 g), and severe (pancreas weight>0.8 g). Normal acinar cells were dominant in the mild pancreases while PanINs and PDAC were dominant in the severe pancreases (Figure 2.13). ACSS2 was most strongly expressed in the severe pancreases and weakest expressed in the mild pancreases (Figure 2.14) suggesting that ACSS2 expression was important in the development of PDAC. Survival analysis revealed that ACSS2-/-KIC mice lived significantly longer than ACSS2+/+KIC mice (Figure 2.15) with a median survival of 80 days for ACSS2-/-KIC mice and 69 days for ACSS2+/+KIC mice. ACSS2+/-KIC mice, with a median survival of 72 days, did not have a statistically significant survival advantage compared with the ACSS2+/+KIC mice (Figure 2.15), suggesting losing one copy of ACSS2 did not provide a significant beneficial effect in PDAC survival.

ACSS2 deficiency might reduce the utilization of fatty acids from pancreas adjacent adipocytes in early PDAC development

The pancreas is a retroperitoneal organ surrounded by adipose tissue. Studies have shown that obesity and adipocytes facilitate the development of PDAC (Incio et al, 2016; Okumuraet al, 2017). In 8 weeks old KIC mice, adipocytes were associated with the ACSS2-

/-KIC pancreases which were relatively normal as well as the ACSS2+/-KIC pancreases where the PanINs were initiating (Figure 2.16). Interestingly, adipocytes were absent from 8 weeks old ACSS2+/+KIC pancreas, which bear more advance PDAC. Adipocytes also seemed absent in regions of more advanced PDAC within ACSS2+/-KIC pancreas (Figure 2.16). ACSS2 was expressed in the adipocytes adjacent to pancreas tissue (Figure 2.17). In ACSS2+/-KIC pancreas, ACSS2-positive early PanINs appeared to develop from regions adjacent to adipocytes. In contrast, regions adjacent to adipocytes in ACSS2-/-KIC pancreas were abounded with normal acinar cells (Figure 2.17).

Discussion

To determine if ACSS2 contributes functionally to the development and progression of PDAC, we genetically ablated ACSS2 function in KIC and KPC mice. We successfully generated ACSS2+/+;KIC, ACSS2+/-;KIC, and ACSS2-/-;KIC that were as similar as possible in terms of genetic background, and then compared PDAC development.

An alternative method is to conditionally ablate ACSS2 using a pharmacological approach. Based on our hypothesis, the pharmacologic inhibition of ACSS2 may affect tumor progression in Kras-driven pancreatic cancer models. We hypothesize that an inhibitor of ACSS2 may have therapeutic value. Mice will also be treated with gemcitabine alone and vehicle as comparators (gemcitabine, 12.5 mg/kg 3x/week ip).

Summary

Elevation of ACSS2 expression in mouse PDAC precancerous lesions suggests that ACSS2 may be functionally important in pancreatic cancer development. Our evidence revealed that the lack of ACSS2 reduces the tumor burden in a genetic, Kras-driven mouse model of pancreatic cancer (KIC). ACSS2 expression in ACSS2+/- tumors is also positively correlated with the tumor size. These promising data suggest that ACSS2 contributes functionally to the development and progression of PDAC. Further investigations of pharmacological inhibition of ACSS2 might represent a therapeutic strategy to inhibit PDAC development or progression.

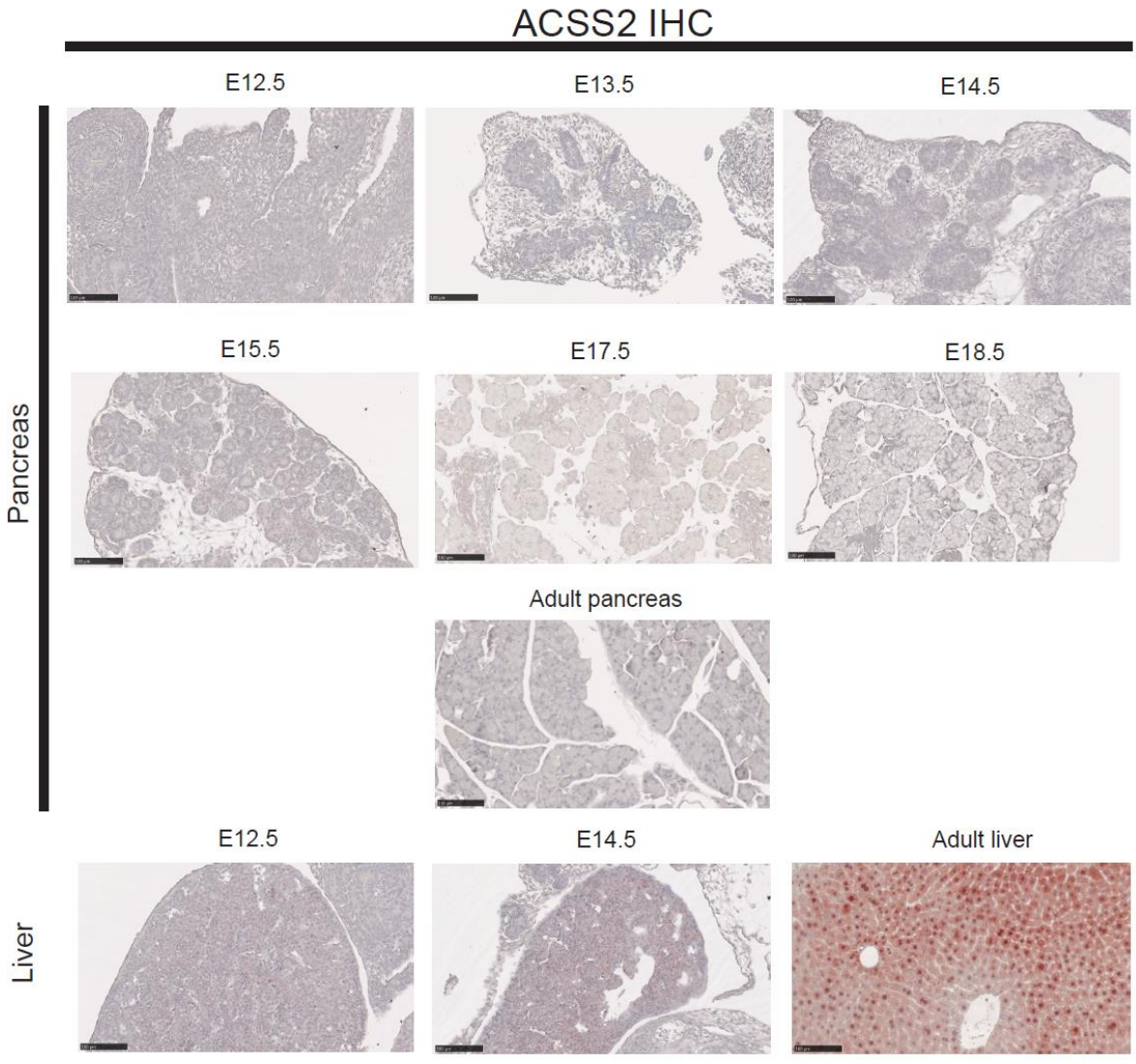

Figure 2.1 ACSS2 expression during the development of pancreas and liver
IHC staining of ACSS2 protein expression in E12.5, E13.5, E14.5, E15.5, E17.5, E18.5, and adult pancreas, and in E12.5, E14.5, and adult liver. Scale bar, 100 μm. ACSS2 did not express in mouse pancreas from E12.5 to adult. ACSS2 expression was evident in liver starting from E14.5.

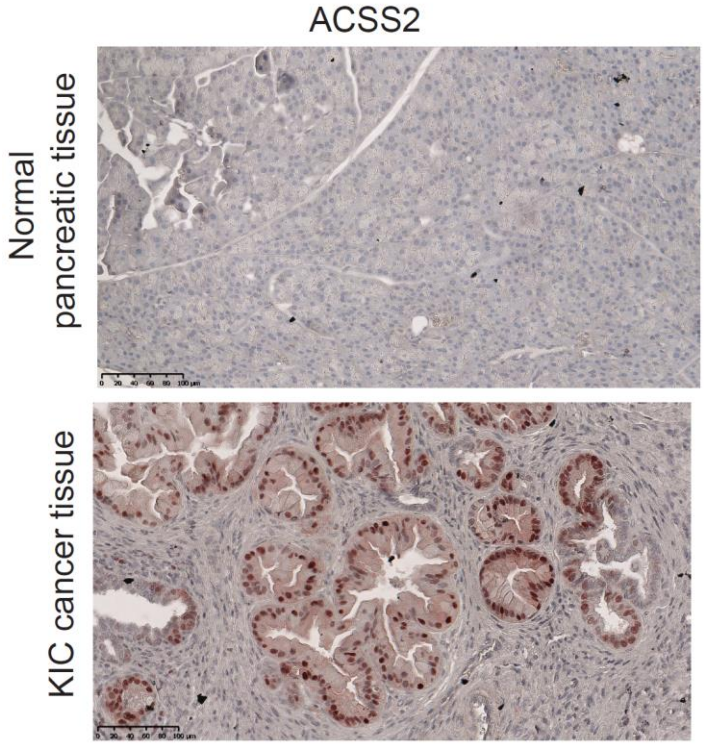

Figure 2.2 IHC staining of ACSS2 protein expression in pancreatic tissue
IHC staining of ACSS2 protein expression in pancreatic tissue from 8-week-old normal or KIC mice. Scale bar, 100 μm. ACSS2 is not expressed in normal pancreatic tissue whereas its expression is elevated in KIC cancer tissue.

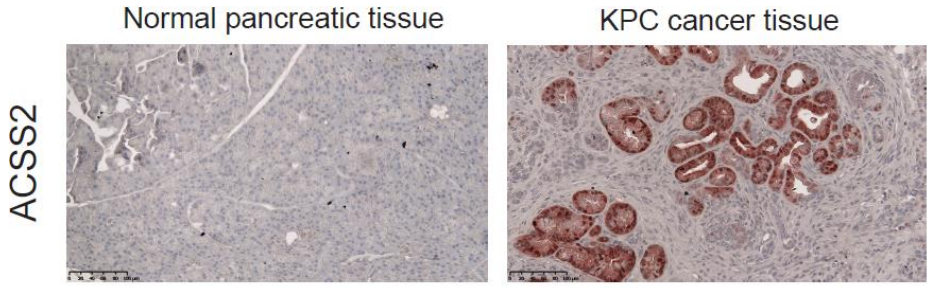

Figure 2.3 IHC staining of ACSS2 protein expression in pancreatic tissue
IHC staining of ACSS2 protein expression in pancreatic tissue from 8-week-old normal or KPC mice. Scale bar, 100 μm. ACSS2 is not expressed in normal pancreatic tissue whereas its expression is elevated in KPC cancer tissue.

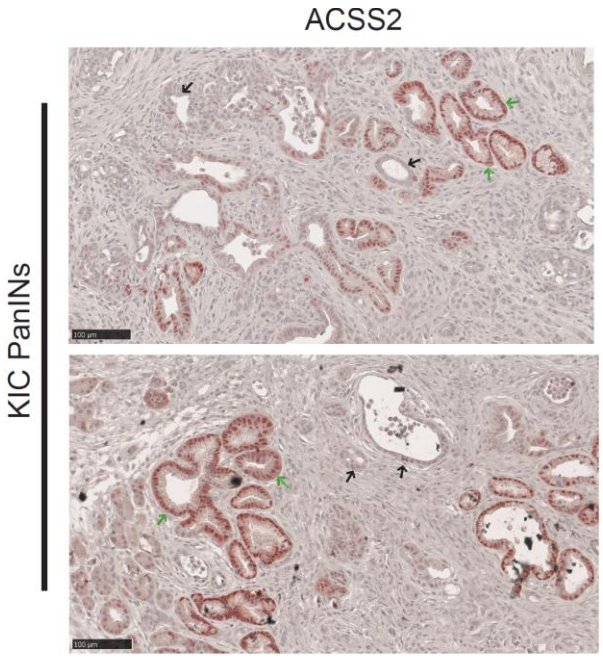

Figure 2.4 The expression of ACSS2 in KIC PanINs
IHC staining of ACSS2 protein expression in pancreatic cancer tissue from 8-week-old KIC mice. Scale bar, 100 μm. The green arrows represent PanIN-1 and 2. The black arrows represent PanIN-3. The expression of ACSS2 in PanIN-3 lesions which have severe cytological and architectural atypia.

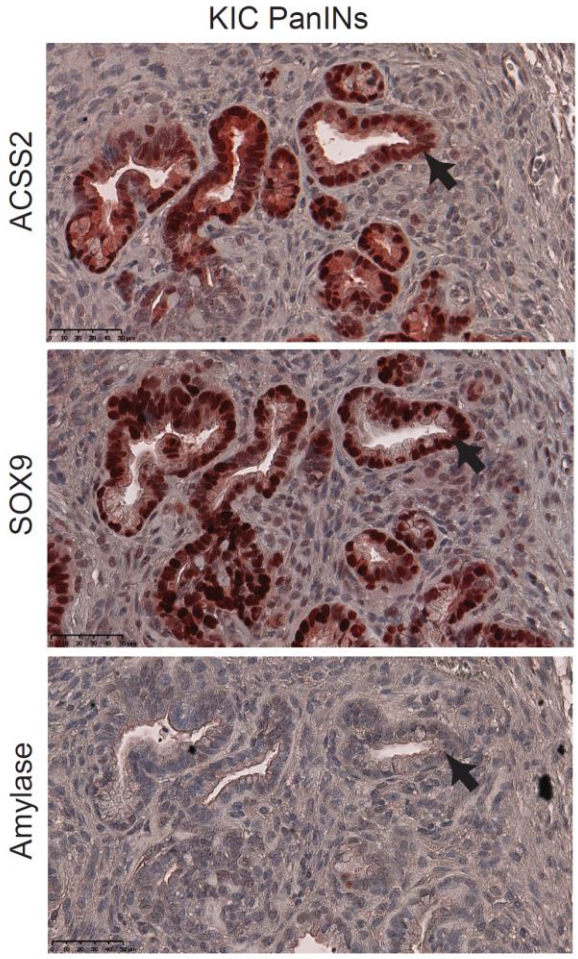

Figure 2.5 IHC staining of ACSS2, SOX9, and Amylase in serial KIC sections.
IHC staining of ACSS2, duct cell marker SOX9 and acinar cell marker Amylase in pancreatic cancer tissue from 8-week-old KIC mice. Scale bar, 100 μm. ACSS2 expression was associated with SOX9 but not Amylase.

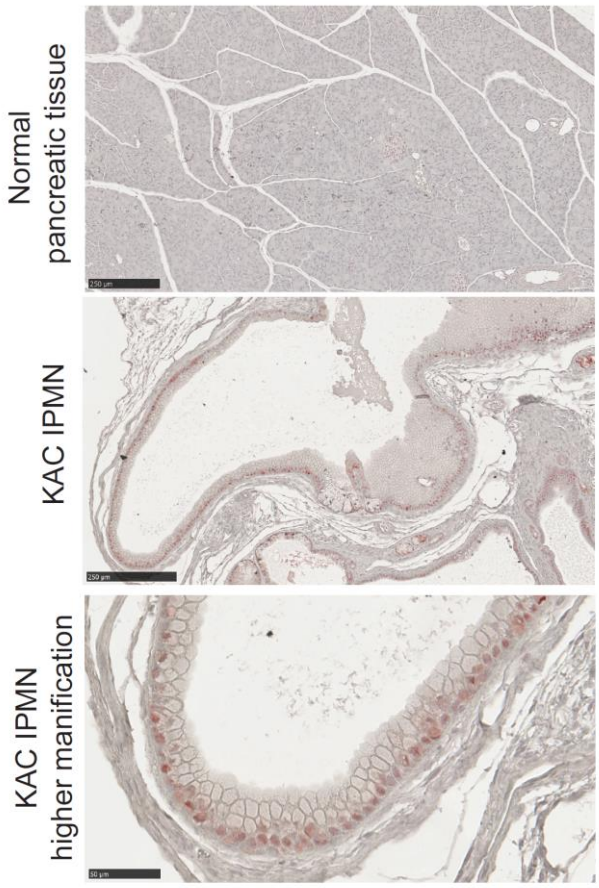

Figure 2.6 IHC staining of ACSS2 in normal pancreas or KAC IPMN
IHC staining of ACSS2 in normal pancreas or $KRAS^{G12D}$; *ARID1A*$^{-/-}$; $P48^{CRE}$ (KAC) IPMN pancreatic cancer tissue. Scale bar, 100 μm. Sections are provided courtesy of Dr. Sam Wang, UTSW. ACSS2 was expressed in the IPMN mouse PDAC model KAC but not normal pancreas tissue, indicating that ACSS2 activation is a common feature of different types of distinct intermediary precursor lesions of PDACs.

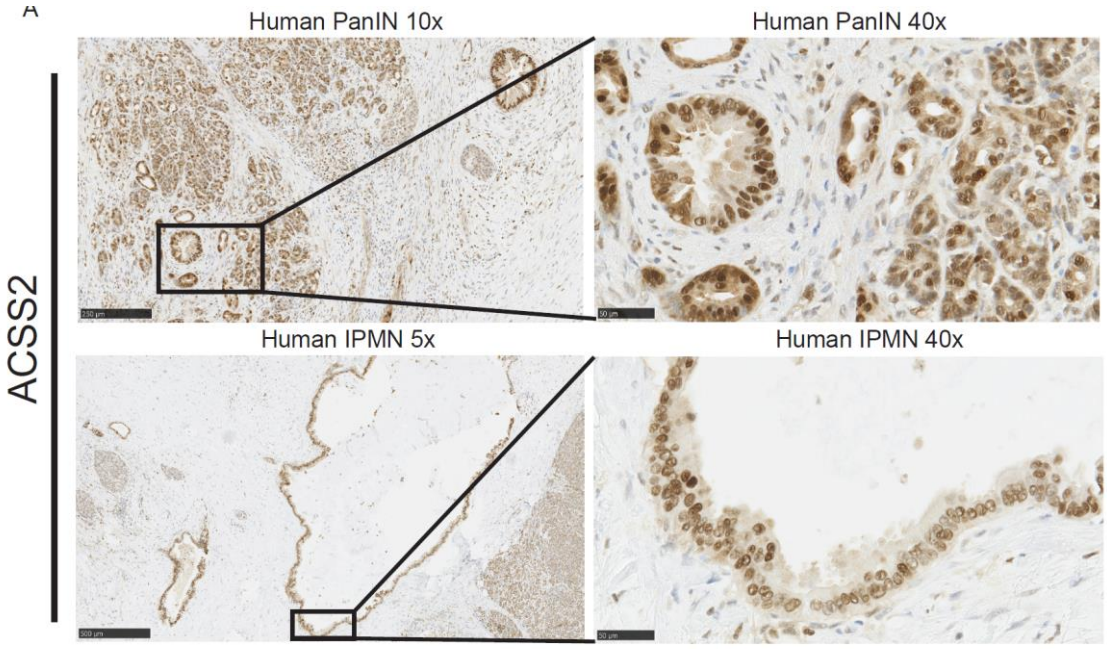

Figure 2.7 IHC staining of ACSS2 in human PanIN and IPMN
Scale bar, 500 μm, and 50 μm. ACSS2 expression was elevated in both PanIN and IPMN in human PDAC.

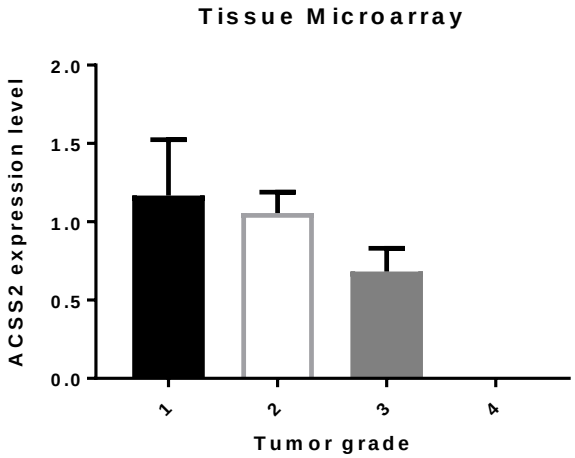

Figure 2.8 Tissue Microarray of ACSS2 expression level in pancreatic tumers
The tissue microarray was constructed from 64 surgically excised human pancreatic ductal adenocarcinomas. IHC staining for ACSS2 was performed on the array which was read by an experienced pathologist Dr. Suntrea Hammer. ACSS2 expression in pancreatic tumor grades 1-4. The expression level of ACSS2 correlated with tumor grade. ACSS2 is highly expressed in tumor grade 1 and 2 but its expression level is reduced in grade 3 and 4.

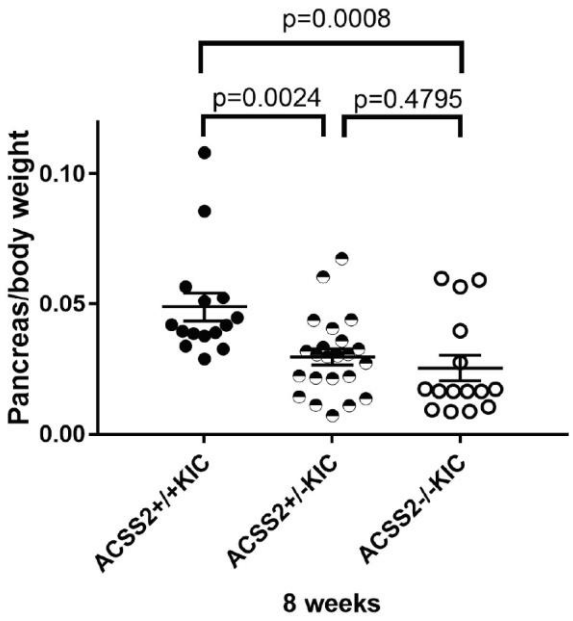

Figure 2.9 Pancreas/body weight of 8-week-old KIC mice
Mass of pancreases from 8-week-old ACSS2+/+ KIC (n=15), ACSS2+/- KIC (n=23) and ACSS2-/- KIC (n=15) mice normalized against body weight. Data represent mean ± SEM. The pancreas/body weight was significantly lower in ACSS2-/- KIC than in ACSS2+/+ KIC mice at 8 weeks of age.

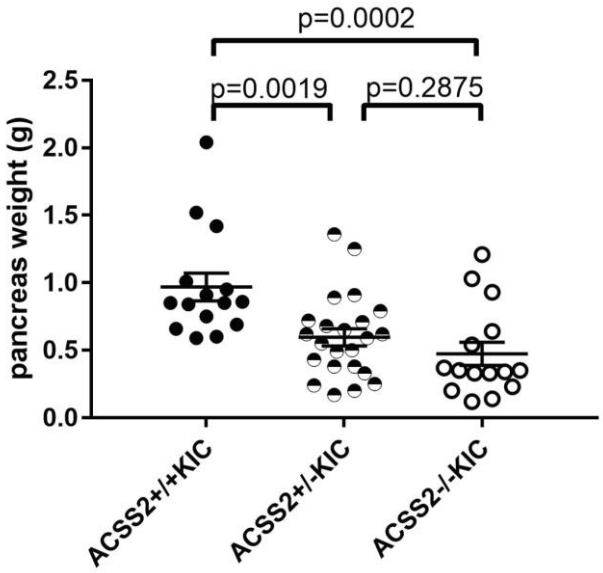

Figure 2.10 Pancreas weight of 8-week-old KIC mice
Mass of pancreases from 8-week-old ACSS2+/+ KIC (n=15), ACSS2+/- KIC (n=23) and ACSS2-/- KIC (n=15) mice were measured upon dissection at 8 weeks of age. Data represent mean ± SEM.

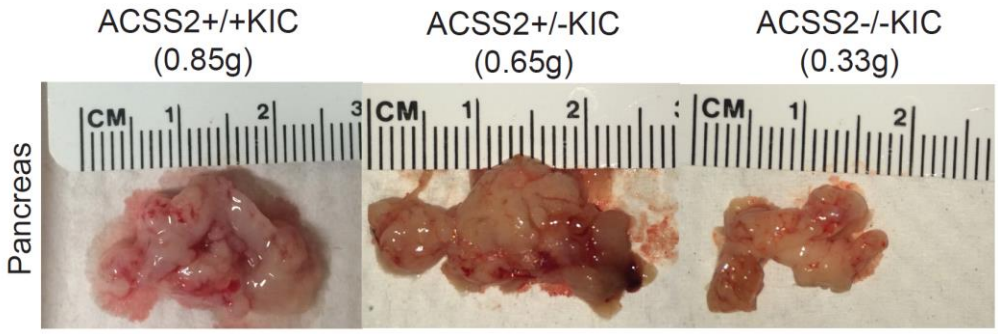

Figure 2.11 The size of pancreas in KIC mice.
General appearance of pancreases from representative ACSS2+/+ KIC, ACSS2+/- KIC and ACSS2-/- KIC mice at 8 weeks of age.

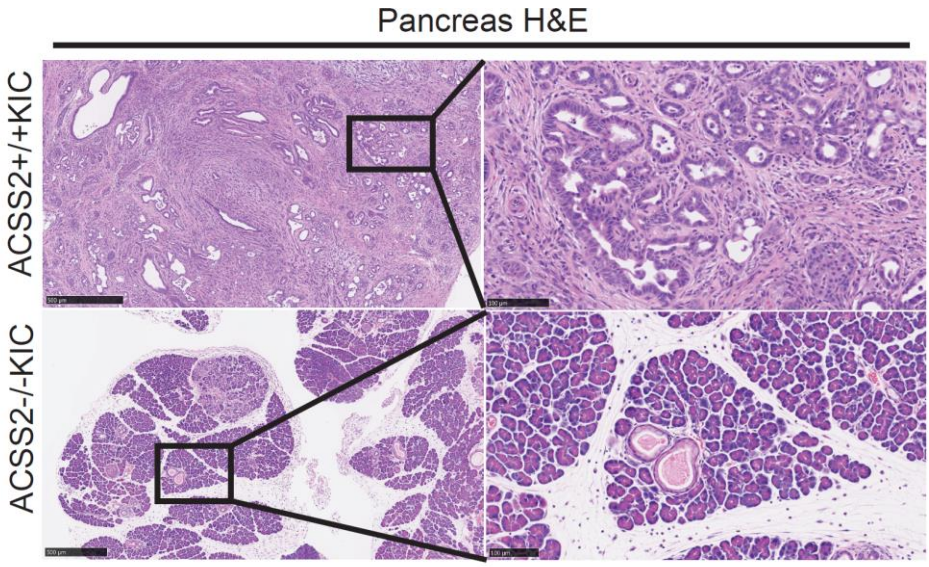

Figure 2.12 Haematoxylin and eosin imaging of pancreases
Haematoxylin and eosin imaging of pancreases from representative ACSS2+/+ KIC and ACSS2-/- KIC of 8 weeks old. Scale bar, 500 μm and 100 μm. At 8 weeks, the ACSS2+/+ KIC pancreases were abounded with PanINs and PDAC, while in ACSS2-/- KIC pancreases, the pancreases were still relatively normal and abounded with normal acinar cells while PanIN-1 start to emerge in a few regions.

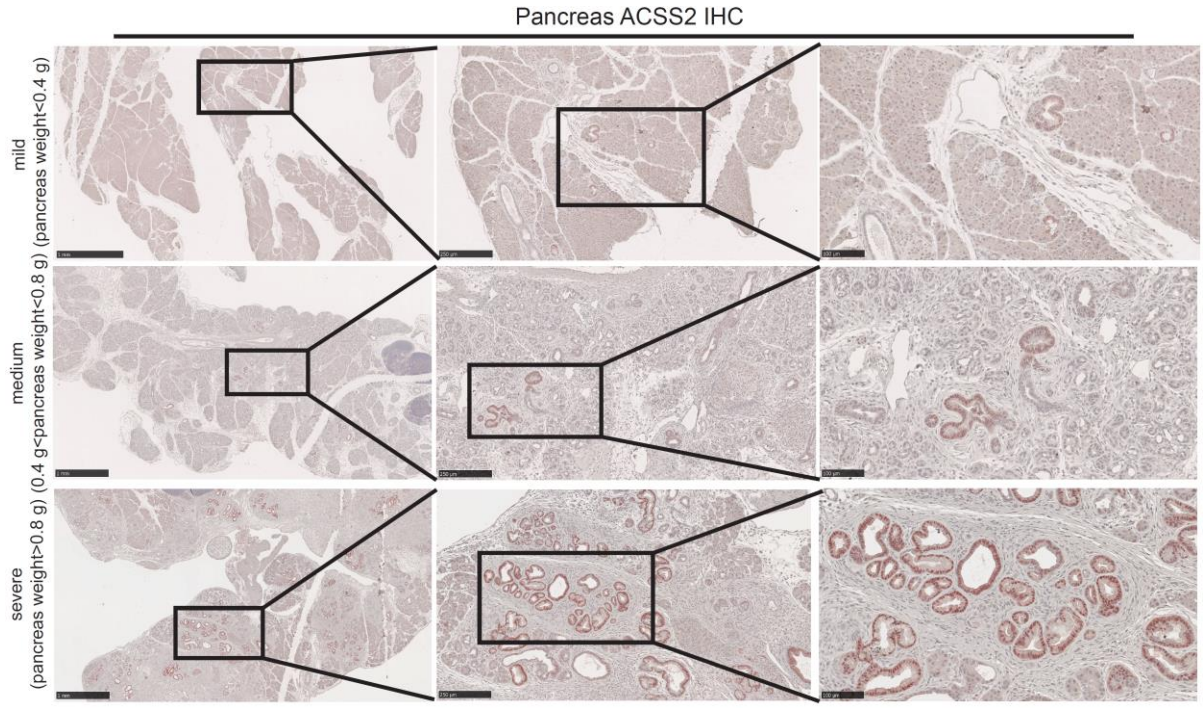

Figure 2.13 IHC staining of ACSS2 in ACSS2+/- pancreases
The pancreases were divided into three groups according to their pancreas weight: mild (pancreas weight < 0.4 g), medium (0.4 g < pancreas weight < 0.8 g), and severe (pancreas weight > 0.8 g). Normal acinar cells were dominant in the mild pancreases while PanINs and PDAC were dominant in the severe pancreases and weakly expressed in the mild pancreases. Scale bar 1 mm, 250 μm, and 100 μm.

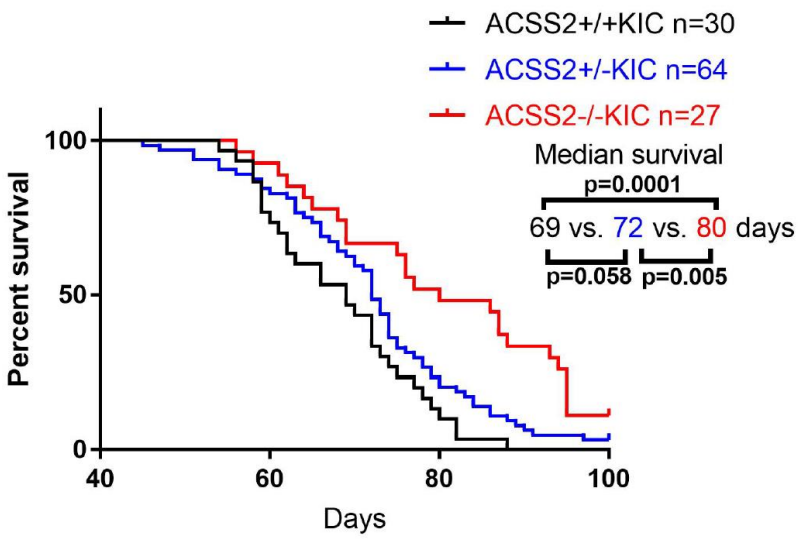

Figure 2.14 Survival analysis of KIC mcie
The survival curve for each group of mice was estimated using the Kaplan-Meier method and the difference in overall survival between the 2 groups assessed by the log-rank test ($P < .0001$). ACSS2+/- KIC mice, with a median survival of 72 days, did not have a statistically significant survival advantage over ACSS2+/+ KIC mice. ACSS2-/- KIC mice lived significantly longer than ACSS2+/+ KIC mice.

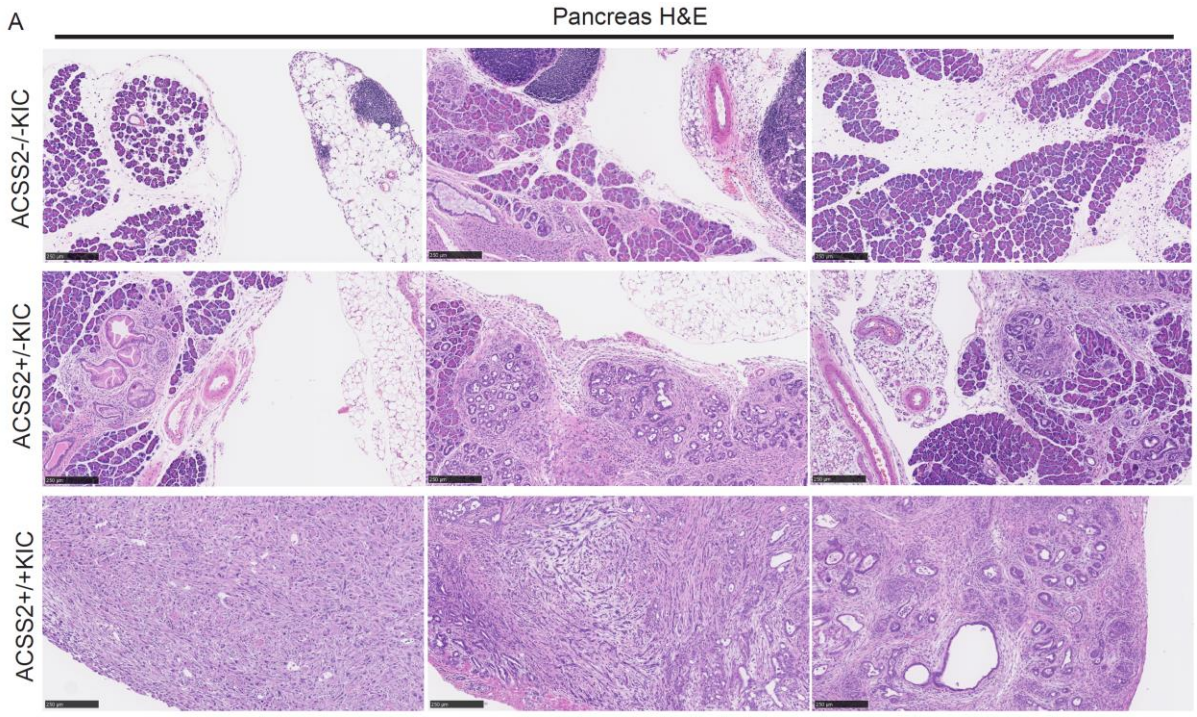

Figure 2.15 Haematoxylin and eosin imaging of pancreases from KIC mice
Haematoxylin and eosin imaging of pancreases from representative ACSS2+/+ KIC , ACSS2+/- KIC, and ACSS2-/- KIC at 8 weeks of age. Scale bar 250 μm. Adipocytes were associated with ACSS2-/- KIC pancreases which were relatively normal and with ACSS2+/- KIC pancreases in which the PanINs were initiating.

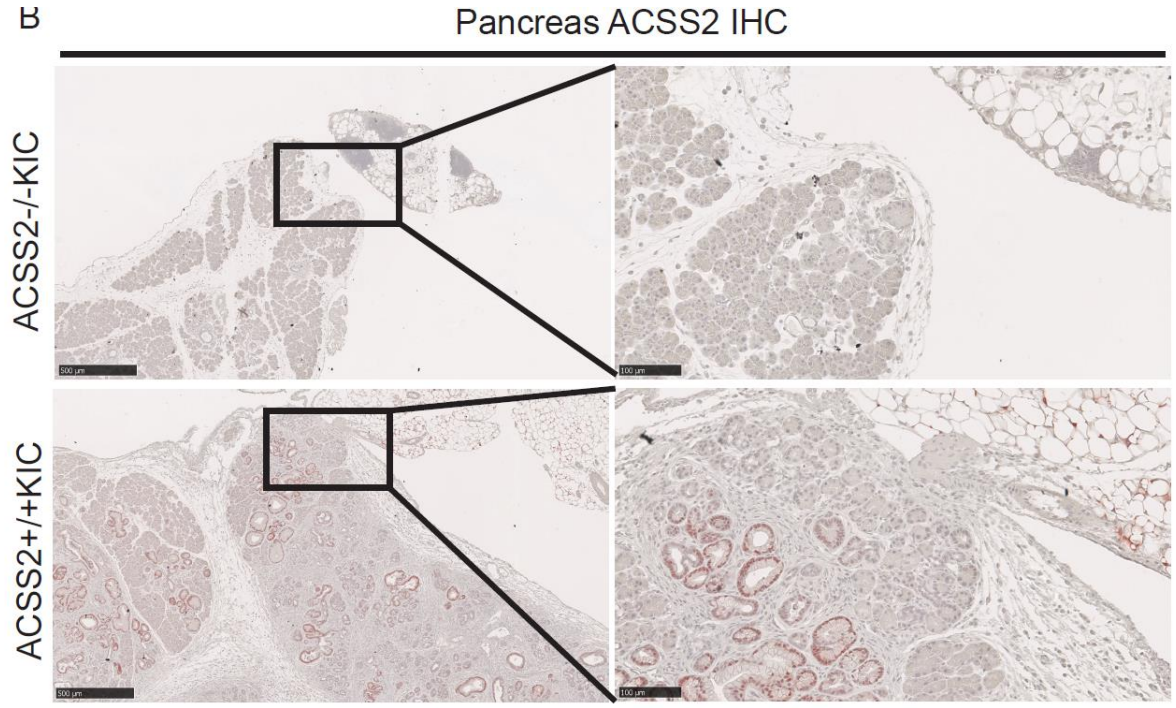

Figure 2.16 IHC staining of ACSS2 in pancreases of KIC mice
IHC staining of ACSS2 in 8-week-old ACSS2+/+ KIC, ACSS2+/- KIC, and ACSS2-/- KIC pancreases. Scale bar 500 μm, and 100 μm. ACSS2 was expressed in the adipocytes surrounding pancreas tissue. ACSS2-/- KIC pancreas was abounded with normal acinar cells.

CHAPTER THREE

Methionine-Responsive Regulation of Protein Phosphorylation Mediated by Protein Phosphatase 2A (PP2A)

Introduction

Protein Phosphatase 2A (PP2A) is the most ubiquitously expressed, tightly regulated serine/threonine phosphatase in all eukaryotic cells (Stanevich et al, 2011; Xu et al, 2006). It plays an important role in many aspects of cellular physiology, including cell cycle, proliferation, development, and regulation of numerous signal transduction pathways. The PP2A holoenzyme comprises a heterodimeric core enzyme, which consists of a scaffold subunit (A subunit) and a catalytic subunit (C subunit), and a variable regulatory subunit (B subunit) (Shi, 2009). Methylation of PP2A is a conserved regulatory mechanism for its function. The methylation is catalyzed by a conserved PP2A-specific enzyme, called leucine carboxyl methyltransferase 1 (LCMT-1) in mammalian cells. Methylation of the C-terminal leucine in a conserved TPDYFL motif of C subunit enhances the affinity of the PP2A core enzyme for certain B subunits (Shi, 2009). This reversible post-transcriptional modification in part controls the activation and substrate specificity of PP2A holoenzyme, thus might be critical to the regulation of PP2A phosphosubstrates. It has been demonstrated that the malfunction of PP2A holoenzymes is closely linked to multiple human diseases, including cancers (Seshacharyulu, 2013) and Alzheimer's disease (Vafai and Stock, 2002; Sontag et al, 2004).

However, the regulation of PP2A methylation is poorly understood. Previously, our lab has discovered the role for methionine in modulating the methylation status of PP2A (Sutter et al, 2013). Methionine boosts synthesis of its downstream metabolite, S-adenosylmethionine (SAM), which functions as the methyl donor for LCMT-1 (Figure 3.1). It is demonstrated in budding yeast that methionine and SAM levels enable cells to sense a key aspect of cellular metabolic state and nutrition availability (Sutter et al, 2013). When yeast are switched from complete to a less rich media without severe nitrogen starvation, yeast induce autophagy to maintain homeostasis and adapt to the new environment. Unexpectedly, a single amino acid, methionine, is sufficient to potently inhibit autophagy under these conditions. Subsequent metabolic analysis indicated that methionine and SAM act as important signals of amino acid sufficiency and regulate cell growth by modulating the methylation status of PP2A (Laxman et al, 2014; Sutter et al, 2013).

Kinetic parameters of LCMT-1-catalyzed methylation of PP2A

To study the methylation of PP2A catalyzed by LCMT-1, I firstly reconstituted the methylation activity of LCMT-1 *in vitro*. LCMT-1 was purified from *E.coli*, PP2A core enzyme was kindly provided by Dr. Yongna Xing at University of Wisconsin Madison. It has been reported that PP2A C subunit alone can be methylated by LCMT-1 *in vitro* (Stanevich et al, 2011). However, I decided to use PP2A core enzyme, which includes both the C and A subunit, because it has been reported that A subunit enhances LCMT-1-mediated methylation of PP2Ac-tail in that the presence of A subunit reduces the K_m of PP2A methylation by 7-

fold (stanevich et al, 2014). The purities of LCMT-1 and PP2A are shown (Figure 3.2). I estimated their purity to be >95%.

An antibody that specifically recognizes methylated PP2A C subunit was used to determine the methylation activity of LCMT-1 by immunoblotting. PP2A-C can be methylated *in vitro* in the presence of LCMT-1 and the methyl donor SAM (Figure 3.3).

I further used liquid chromatography–mass spectrometry system to determine the kinetic parameters of LCMT-1-catalyzed methylation of PP2A-C (Figure 3.4). The K_m of SAM was determined to be $1.86 \pm 0.11\,\mu M$, which is comparable for the K_m values of other SAM-dependent enzymes. SAH (S-adenosylhomocysteine, a known inhibitor of SAM-dependent methyltransferases) has a K_i of ~ 0.07uM, which is unusually low among SAM-dependent methyltransferases (Table 3.1). This strongly suggests that LCMT-1 is easily inhibited by low concentrations of SAH and would be very responsive to the intracellular SAM/SAH ratio.

Methionine deprivation study in cell lines

293T cells and U2OS cells were deprived of methionine followed by a methionine rescue. An antibody that targets unmethylated form of PP2A-C was used to determine the methylation level of PP2A-C. During methionine deprivation, in both cell lines the methylation level of PP2A decreased, while the amount of total PP2A (methylated + unmethylated) did not change. PP2A methylation was rescued upon adding back methionine. Furthermore, LC-MS results show that SAM levels decreased upon methionine deprivation and increased after methionine was added back, which followed a similar trend as PP2A

methylation amounts. This indicates that SAM may act as a signal of amino acid sufficiency and modulate the methylation status of PP2A.

Upon methionine deprivation, 293T cells did not show a decrease in histone methylation levels, indicating that PP2A methylation is much more sensitive to methionine/SAM availability than histone methylation (Figure 3.5).

Methionine deprivation in mice

To investigate the effect of methionine deprivation *in vivo*, I conducted a methionine deprivation study in C57BL/6 mice. 2 mice were put on chow diet while 3 were on s methionine and choline depleted diet for one week. Blood and organs were collected upon dissection. No difference was found in PP2A methylation level in liver or heart between the two groups of mice (Figure 3.6). Serum levels of methionine were .? This preliminary experiment suggests that one week of a methionine-restricted diet might not be sufficient to significantly reduce free circulating methionine levels.

SILAC phosphoproteomics experiment comparing WT vs. *ppm1*Δ cells

In collaboration with Dr. Yonghao Yu, we conducted a SILAC (Stable Isotope Labeling by Amino Acids in Cell Culture) phosphoproteomics experiment to compare WT yeast cells vs. *ppm1*Δ cells lacking the yeast PP2A methyltransferase. We identified nearly 90,000 phosphopeptides. The ratio (WT/*ppm1*Δ) of each detected phosphopeptide is shown in the scatter plot (Figure 3.7). The distribution curve is expectedly symmetrical, displaying roughly an equal number of phosphopeptides significantly enriched in WT cells (left side of

plot), and phosphopeptides significantly enriched in the *ppm1*Δ mutant cells (right side of the plot). The majority of detected phosphopeptides exhibited minimal change in WT vs. *ppm1*Δ (log_2ratio ~ 0, middle of plot).

The dataset not only indicates changes in phosphopeptide abundance but also the corresponding positional sites of modification. GO (Gene Ontology) analyses of those phosphopeptides with WT/*ppm1*Δ ratio > 2.8, or < 0.35, reveal that many different functional categories of proteins are influenced by Ppm1p and methylated-PP2A. Notably, phosphopeptides of proteins involved in signal transduction and protein phosphorylation tend to be increased in WT relative to *ppm1*Δ cells, while many phosphopeptides of proteins involved in transcription, cellular response to stimulus, and endocytosis tend to be increased in *ppm1*Δ relative to WT. In particular, those phosphopeptides that increase in abundance in *ppm1*Δ mutant cells relative to WT might be candidates for direct substrates of methylated-PP2A.

ITC experiments studying the interaction between LCMT-1 or PPM1 with SAM or SAH

To investigate the biochemical basis of how PP2A methylation is responsive to the SAM/SAH ratio, I conducted an isothermal titration calorimetry (ITC) experiment to compare the binding affinity of SAM or SAH to LCMT-1 or PPM1. Both methyltransferases showed no difference in the binding affinity for SAM compared to SAH. The thermodynamic parameters are as shown in Figure 3.8. The results revealed that the sensitivity of PP2A

methylation to SAM/SAH might not simply be due to differences in binding affinity between SAM and SAH.

High-throughput screen for LCMT-1 inhibitors

The above evidence showed that the K_i for SAH is unusually low, especially compared to histone lysine methyltransferases (Patnaik et al, 2004; Chin et al, 2006). This supports the hypothesis that the methylation of PP2A is responsive to the intracellular SAM/SAH ratio, and potentially qualifies the LCMT-1 enzyme to be a "SAM sensor". Therefore, inhibitors of LCMT-1 will be particularly useful for interrogating the role of this SAM-responsive methylation of PP2A in a variety of cell types without genetic manipulation.

The methylation modification on PP2A is chemically quite different (methylesterification, O-Me bond), compared to lysine (N-Me) or nucleic acid (C-Me, N-Me) methylation. So there is no reason a priori to assume that all inhibitors obtained will be pan-inhibitors. In fact, the distinctive reaction mechanism of LCMT-1 strongly suggests inhibitors specific to LCMT-1 can be obtained. Dr. Noelle Williams has conducted a high-throughput screen for DNMT1 inhibitors. I tested their top DNMT1 hit SW155246 and it does not inhibit LCMT-1 as assayed using the RapidFire LC-MS system (Figure 3.9).

I conducted a high-throughput screen for small molecule inhibitors of LCMT-1 (Figure 3.10). The screen was carried out with the help of the UTSW high-throughput screening Core Facility. The UTSW chemical library consists of over 200,000 compounds as well as over 40,000 natural product fractions contributed by Dr. John MacMillan.

I firstly performed a mock plate run showing the screen is indeed ready to go (Figure 3.11). Those hits with robust Z score < -3 were determined as inhibitors, and robust Z score > 3 as activators. I then conducted 3 screens including 11k compounds. Among the 6 hits of potential inhibitors, 4 have been re-tested by immunoblotting. I found one molecule, named palonosetron, showed an inhibition on LCMT-1 with an approximately IC50 of 3 μM (Figure 3.12).

Discussion

In eukaryotic genomes, genes that encode protein kinases outnumber by two- to threefold genes that encode protein phosphatases (Fellner et al, 2003). To counter balance the activity of the substrate-specific kinases, phosphatases form holoenzymes via different combinations. The mechanism of how PP2A acquires its intracellular specificity and activity is poorly understood.

Previous study in our lab revealed that in budding yeast methionine is a key signal of amino acid sufficiency. Methionine inhibits autophagy and promotes growth by inducing methylation of PP2A on the very C-terminus of its catalytic subunit. The methylation of PP2A promotes the dephosphorylation of Npr2p, a component of a conserved complex that inhibits TORC1. Dephosphorylated Npr2p is unable to inhibit TORC1 signaling, thus blocking autophagy. Therefore, the methylation of PP2A functions to promote growth and inhibit autophagy in response to amino acid sufficiency. We hypothesize that the methylation of PP2A catalyzed by LCMT-1 in mammalian cells or by PPM1 in yeast plays an important role in the regulation of its substrate specificity and activity.

The evidence in this study indicates that LCMT-1 is very sensitive to the SAM/SAH ratio. The low K_i for SAH poises LCMT-1 to be a "SAM sensor" *in vivo*. Moreover, an another independent study carried out by the Cravatt lab showed that PP2A methylation decreased substantially upon overexpression of NNMT methyltransferase, which consumes methyl units from SAM (Ulanovskaya et al, 2013). Their finding further supports our hypothesis that the methylation of PP2A is sensitive to SAM availability.

The precise mechanism of how LCMT-1 senses SAM/SAH level remains unclear. ITC result indicates that the binding affinities of SAM and SAH on LCMT-1 are similar, both with a Kd in the micromolar range. However, since the binding affinities were measured *in vitro* in the absence of PP2A, they may not be reflective of the real affinities and interactions *in vivo*. The presence of PP2A and other intracellular proteins, and perhaps the local cellular environment, may contribute to the sensitivity of LCMT-1 to SAH.

Summary

PP2A plays an important role in many aspects of cellular physiology. However, the regulation of PP2A methylation is poorly understood. Methylation of PP2A is catalyzed by a PP2A-specific enzyme, LCMT-1. I have reconstituted the methylation activity of LCMT-1 in vitro and determined the kinetic parameters of LCMT-1-catalyzed methylation of PP2A. I found that LCMT-1 might be a "SAM sensor" as it is very sensitive to the SAM/SAH ratio. Methionine deprivation study in cell lines revealed that methionine depletion boosts PP2A demethylation. It indicates that methylation of PP2A may play a critical role in regulating cell growth and autophagy. I further conducted a high-throughput screen to identify potent

and specific small molecule inhibitors of LCMT-1. The inhibitors of LCMT-1 will be useful for determining the role of this methionine-responsive phosphatase in cells and for investigating the phosphoproteome network regulated by the methylation level of PP2A.

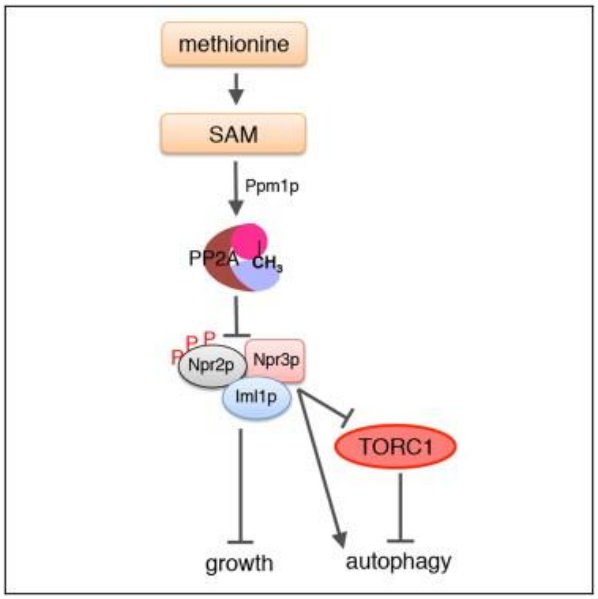

Figure 3.1 Methionine boosts the synthesis of SAM, which functions as the methyl donor for Ppm1.
Model depicting how the methylation of PP2A, catalyzed by Ppm1p (LCMT-1 in mammals), functions to inhibit autophagy and promote growth. Methylated-PP2A promotes dephosphorylation and inactivation of Npr2p (an inhibitor of TORC1), but also has many other substrates.

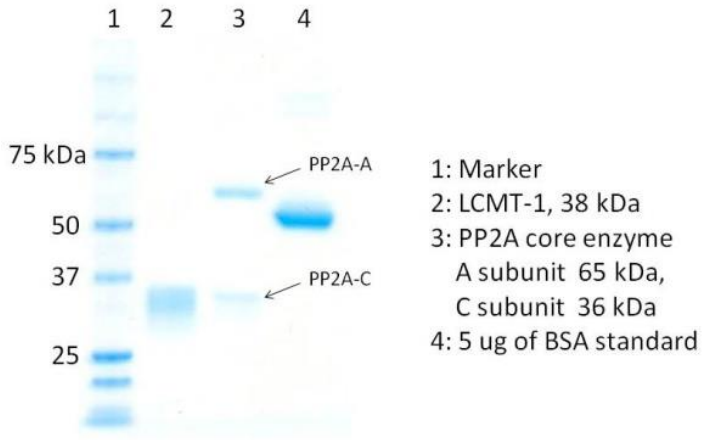

Figure 3.2 Purified LCMT-1 and its protein substrate PP2A
Final purified fractions of LCMT-1 and PP2A-A + C subunits are shown next to a BSA standard to assess purity.

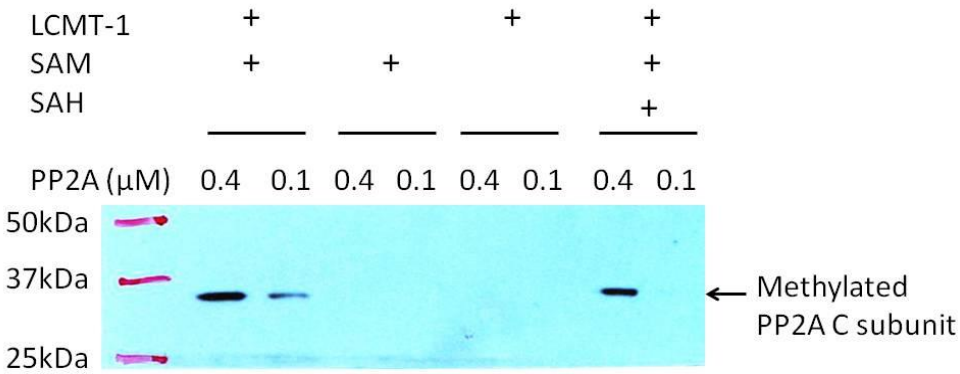

Figure 3.3 *In vitro* methylation of PP2A
PP2A core enzyme can be methylated *in vitro* in the presence of LCMT-1 and SAM. The methylation activity of LCMT-1 is inhibited by SAH.

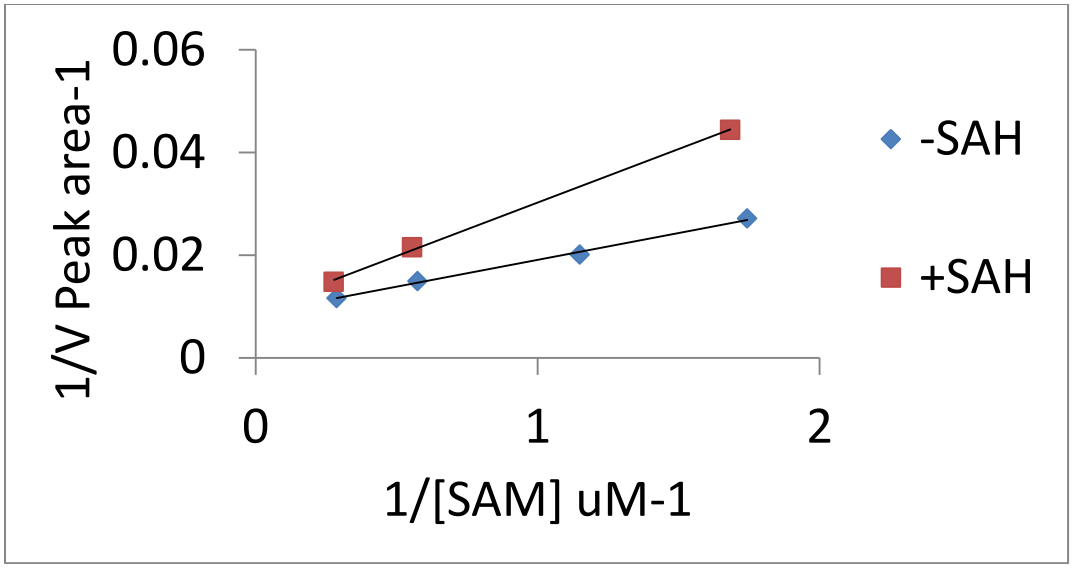

Figure 3.4 Enzyme kinetics of LCMT-1.
The K_m for SAM is determined by fitting rates with the Michaelis-Menten equation using LC-MS data. The K_m of SAM was determined to be ~1.3 μM. SAH has a K_i of ~80 nM.

Methyltransferase	**K_i for SAH**
m^2-guanine methyltransferase I	8 uM
m^2-guanine methyltransferase II	0.3 uM
m^1-adenine methyltransferase	2.4 uM
cytosine-5-methyltransferase	14.2 uM
tRNA guanine-N-2-methyltransferase	23 uM
Phosphatidylethanomine methyltransferase	3.8 uM
Carboxyl Protein S-isoprenylcysteine	9.2 uM

Table 3.1 K_i for SAH of different methyltransferases.

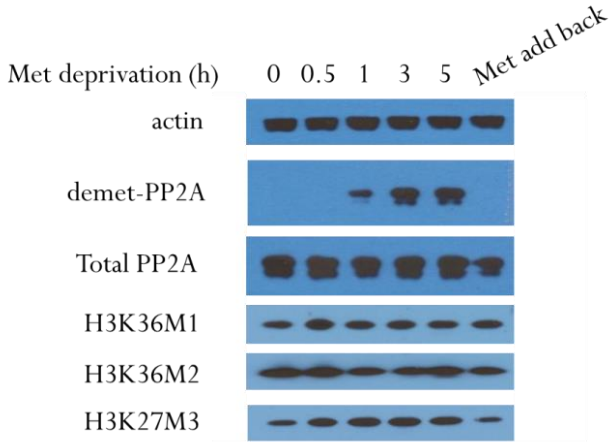

Figure 3.5 Methionine deprivation study in cell lines.
293T cells were deprived of methionine for 0, 0.5, 1, 3, 5 h or 5 h followed by 2 h methionine rescue.

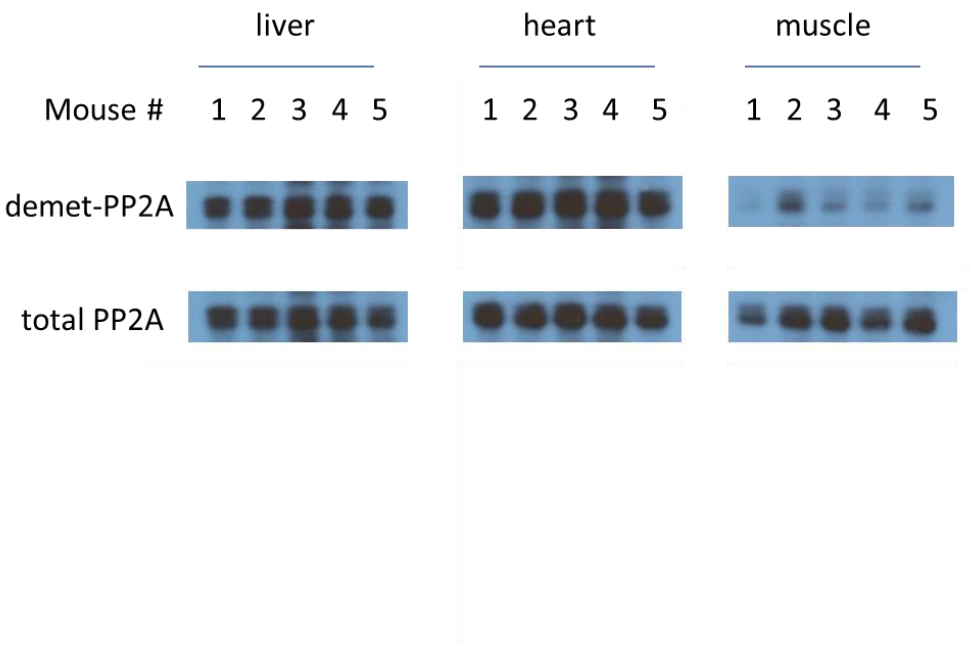

Figure 3.6 Methionine deprivation study in mice
Mice #1 and 2 were put on chow diet while mice #3, 4, and 5 were on methionine and choline depleted diet for one week. Blood and organs were collected following dissection.

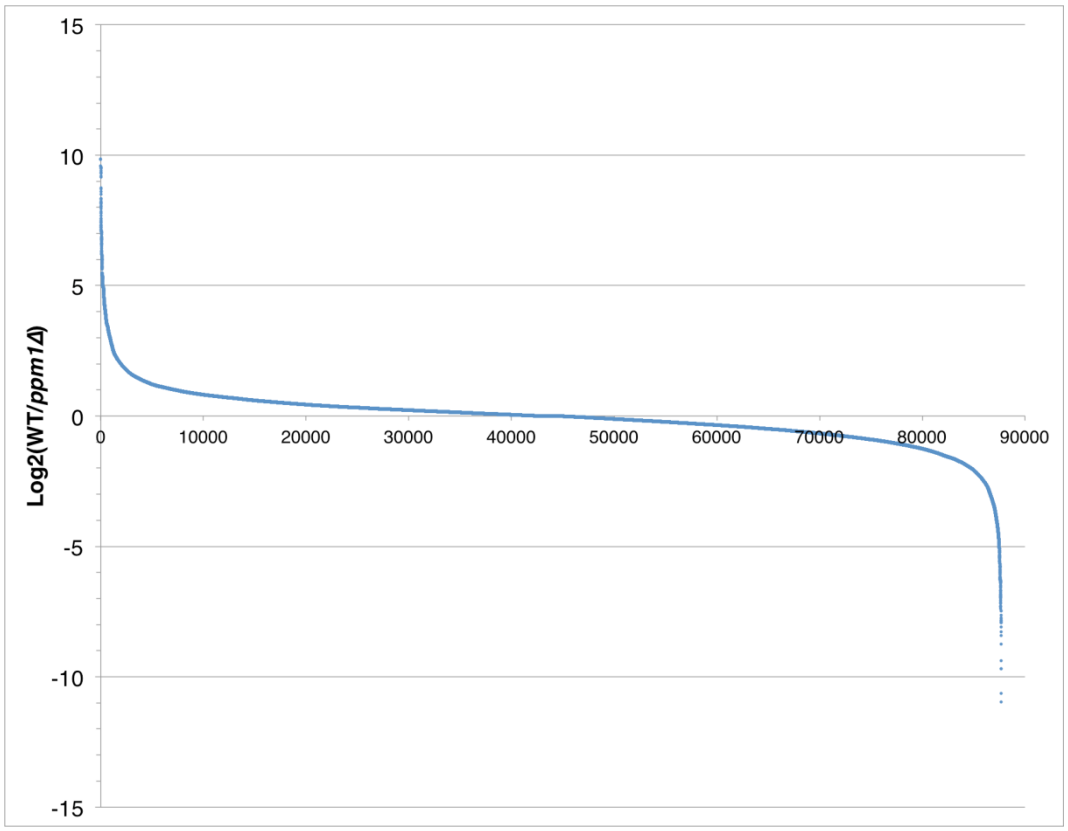

Figure 3.7 SILAC phosphoproteomics experiment comparing WT vs. *ppm1*Δ cells
Phosphopeptides altered in WT vs *ppm1*Δ mutants. Scatter plot showing detection of almost 90,000 phosphopeptides. Each dot along the x-axis represents a single phosphopeptide. Y-axis denotes the ratio of each phosphopeptide in WT vs. *ppm1*Δ (expressed as $\log_2$ ratio).

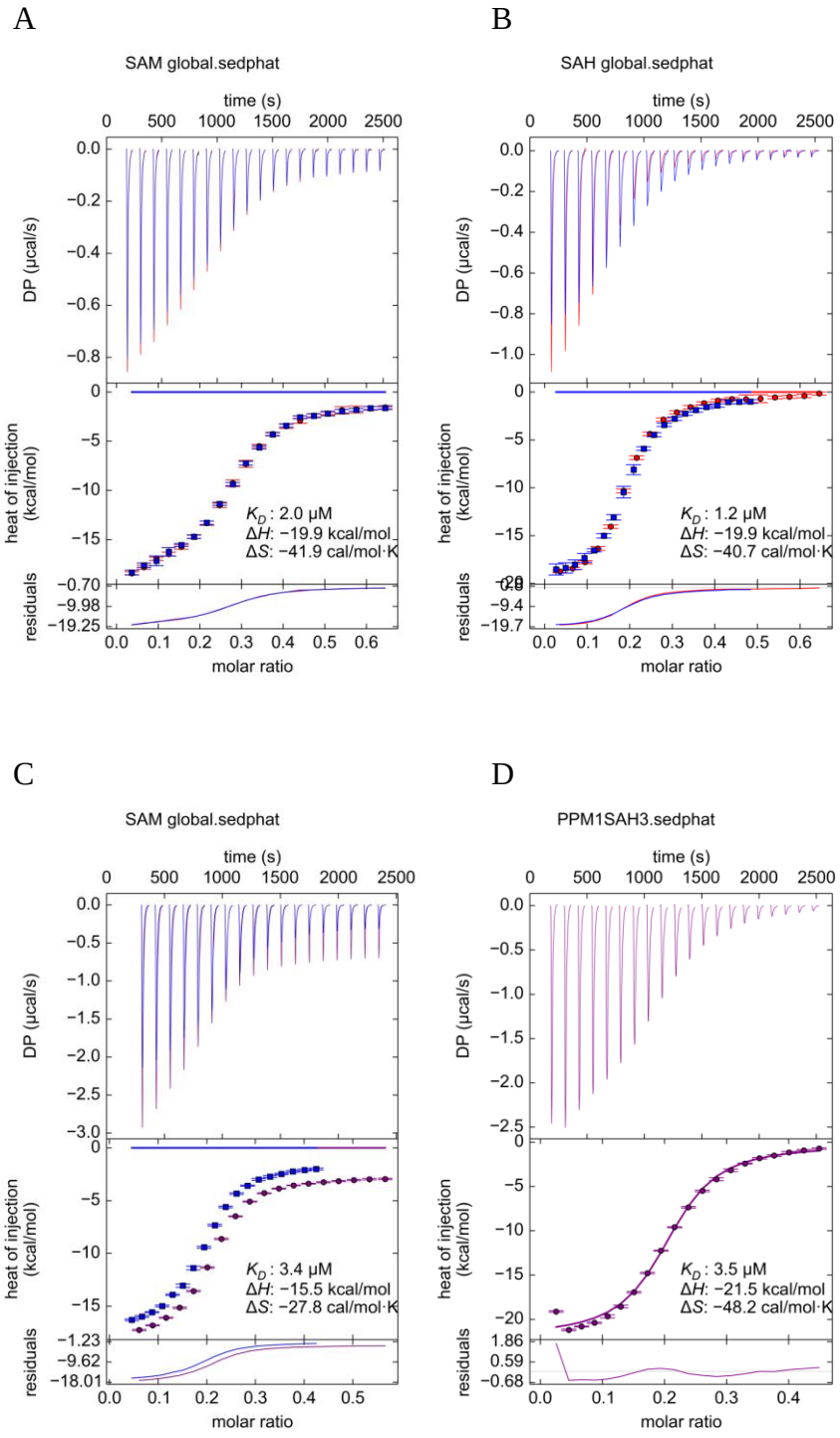

Figure 3.8 ITC experiments studying the interaction between LCMT-1 or PPM1 with SAM or SAH

ITC analysis of SAM (A) or SAH (B) binding to LCMT-1, and SAM (C) or SAH (D) binding to PPM1.

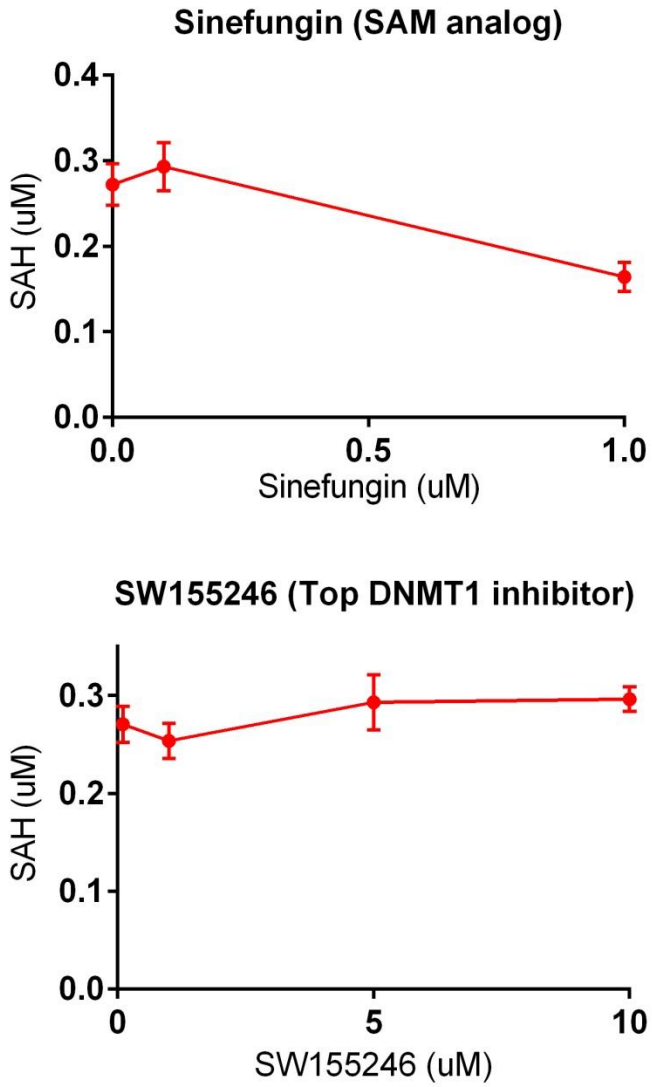

Figure 3.9 Specific inhibitor of DNMT1 does not inhibit LCMT-1
LCMT-1 was mixed with PP2A core enzyme, SAM, and inhibitors. The production of SAH was measured using RapidFire. Sinefungin, which is a SAM analog, was used as a positive control for LCMT-1 inhibitor.

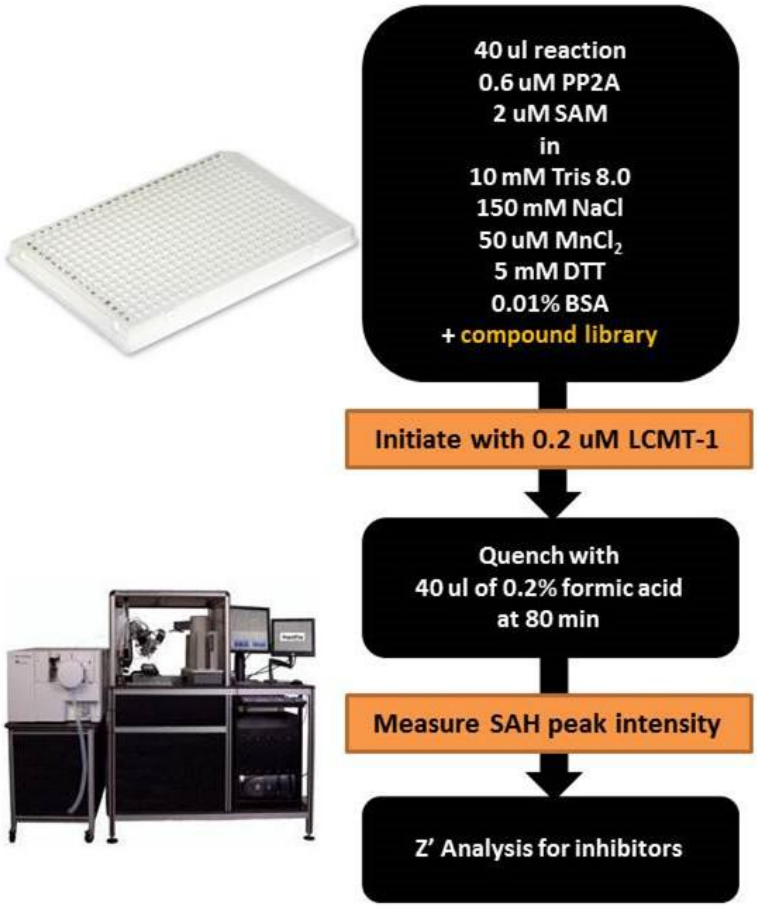

Figure 3.10 Flow chart depicting the proposed high-throughput screen for inhibitors of LCMT-1.
Hits with robust Z score < -3 are determined as inhibitors, and robust Z score > 3 as activators.

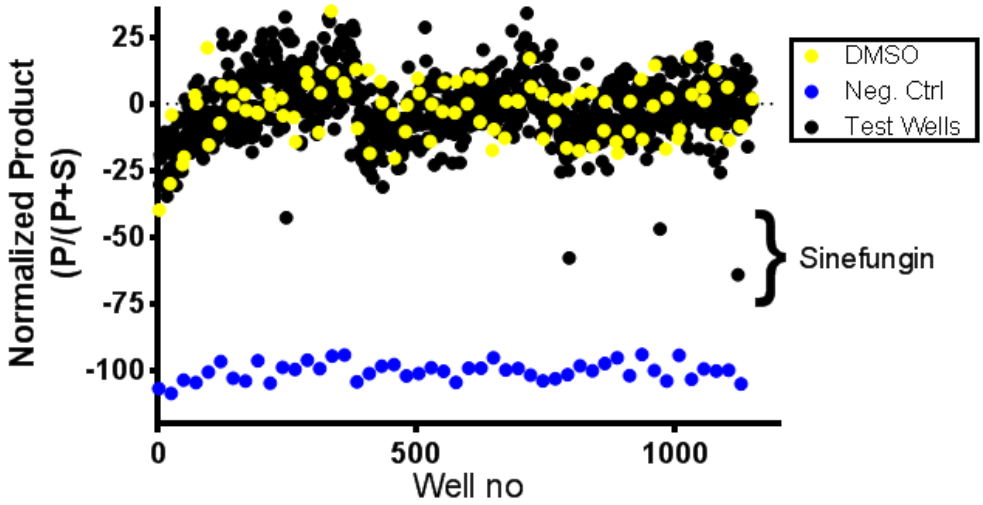

Figure 3.11 A mock plate run
A mock plate run of three 384-well plates was conducted under optimized assay conditions. After quenching the reaction, samples from all plates were read using the RapidFire 300. These results were expressed as an extent of reaction (Product/(Product + Substrate), P/(P+S)), loaded into GeneData's Screener software, normalized, and scaled such that 0 represents no effect, values above 0 represent an activation of enzyme activity, and values less than 0 represent inhibition of enzyme activity. No plate effects were observed for these plates. Wells spiked with the pan-methylase inhibitor sinefungin are indicated in the graph. Other symbols are as follows: DMSO control wells (columns 2, 23), yellow symbols; negative control (column 1), blue symbols; and test wells (DMSO only for mock run), black symbols. The Z' value for all plates was ~0.53.

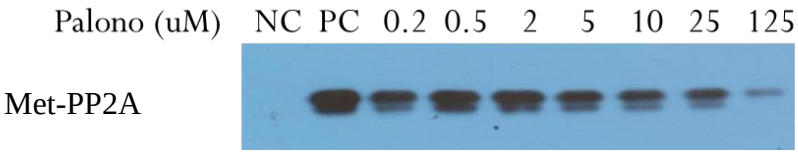

Figure 3.12 Palonosetron inhibits the methylation activity of LCMT-1
The inhibition of palonosetron on LCMT-1 was determined by immunoblotting using an antibody that targets methylated PP2A. Under the condition of 0.6 μM PP2A and 0.06 μM of LCMT-1, the IC50 of palonosetron is ~3 μM.

CHAPTER FOUR

Material and Methods

Mouse studies

All experiments involving animals were conducted under the auspices of the UTSW Animal Care and Use Committee. The generation of ACSS2+/- and ACSS2-/- mice was previously described (Comerford et al, 2014). For diet-induced obesity studies, 9-week-old littermate ACSS2+/+, ACSS2+/-, ACSS2-/- mice were fed a chow (ENVIGO 2016S) or high-fat diet (ENVIGO TD.03584) for 10 to 12 weeks. For intestinal lipid uptake study, mice were fasted overnight. The animals were then orally gavaged with 200 µl olive oil and euthanized either before (control) or 90 min after gavage. The intestine was resected from the ligament of Treitz to the ileocecal junction, divided into proximal, middle, and distal segments of equal length, washed with cold saline, and the jejunum segment was processed for frozen sectioning and ORO staining using standard protocols. For the fasting study, mice were individually caged and fasted for 48 h, anesthetized with isoflurane, exsanguinated by cardiac puncture, and blood and tissues collected for subsequent studies.

Serum metabolite measurements

Serum cholesterol was measured with Cholesterol E kit (439-17501, Wako, Japan). Serum triglyceride level was measured with the L-type Triglyceride kit (461-09891, Wako, Japan). Serum phospholipids level was measured with Phospholipids C kit (433-36201, Wako, Japan). Serum glucose was measured with Autokit glucose (439-90901, Wako, Japan). Serum NEFA was measured with HR series NEFA kit (995-34791, Wako, Japan). Serum

ketone bodies was measured with Total Ketone bodies kit (415-73301, Wako, Japan). Serum insulin was measured with Ultra sensitive mouse insulin ELISA kit (90080, Crystal Chem, IL). Measurements were performed according to the manufacturers protocol.

Glucose tolerance test (GTT)

Mice were fasted overnight for 16 h. Glucose at 1.5 g/kg in saline was injected intraperitoneally and a drop of blood was collected from a tail nick. Glucose was measured at 0, 15, 30, 60, and 120 min post injection using a glucometer (Bayer, Pittsburgh, PA).

Insulin tolerance test (ITT)

Mice were fasted for 4 h. Insulin (Fisher, Hampton, NH) at 0.8 U/kg in saline was injected intraperitoneally and a drop of blood was collected from a tail nick. Blood glucose was measured at 0, 15, 30, 60, and 120 min post injection using a glucometer (Bayer, Pittsburgh, PA).

Histopathology and Immunohistochemistry

Formalin-fixed paraffin-embedded tissue sections were either stained with hematoxylin and eosin (H&E) for routine histological evaluation or left unstained for immunohistochemistry (IHC). The protocol for IHC was previously described6. The antibodies used in the IHC were ACSS2 (Cell Signaling, cat#3658), Fabp1 (Sigma-Aldrich, cat#HPA028275). OCT-embedded frozen tissues sections were stained by Oil O Red according to a standard protocol and also stained with H&E. Slides were scanned on a

NanoZoomer microscopic slide scanner (Hamamatsu Photonics, Hamamatsu, Japan). Images were captured using NDP view software (Hamamatsu Photonics, Japan). Some images were taken with a conventional microscope instead of with the scanner.

Body composition measurement

Body composition of mice, including fat mass and lean tissue mass, were measured by Bruker Minispec mq10 (Bruker, Billerica, MA). Briefly, a mouse was placed in an acrylic cylinder (48-mm diameter) and loosely restrained within the cylinder by pushing a plunger to maintain the animal within a length of 20 cm inside the cylinder dependent on the size of the animal. The cylinder is then positioned inside the bore of the magnet. Measurements of fat and lean mass were recorded and animals returned to their home cage in 1 min.

Hepatic triglyceride extraction

50 mg of liver tissue was homogenized in 0.5 ml PBS. 0.4 ml homogenate was added into 1.6 ml of Chloroform/methanol, 2:1, v/v mixture, and mixed completely by shaking vigorously. The suspension was centrifuged at 3,000 rpm for 10 min at room temperature. The lower organic phase was transferred to clean tubes and air-dried in a chemical hood overnight. The residual liquid was resuspended in 500-2000 μl of 1% Triton X-100 in absolute ethanol, and the concentrations of triglyceride were determined using the L-type Triglyceride kit (461-09891, Wako, Japan). Triglyceride levels were normalized to tissue mass.

Real-time PCR analysis

Total RNA from frozen liver and intestine mucosa was extracted using TRIzol reagent (Invitrogen, Carlsbad, CA). cDNA was synthesized from 2 μg total RNA with High Capacity cDNA Reverse Transcription Kit (Applied Biosystems, Foster City, CA). Real-time PCR primer sequences are included in the Table S1. Each qRT-PCR was analyzed in duplicate and contained in a final volume of 10 μl: 25 ng of cDNA, each primer at 150 nM, and 5 μl of 2× SYBR Green PCR Master Mix (Applied Biosystems, Foster City, CA). Results were evaluated by the comparative cycle number at threshold method 23 using cyclophilin as the invariant reference gene.

Fecal lipid measurement

Mice were individually housed for 15 days. Food intake and body weight were measured every day. Feces were collected every three days and then dried, weighed, and ground. One gram of ground feces was dissolved in 40 ml of Folch solution (chloroform: methanol=2:1) overnight. Solution was filtered with #2 filter paper and filled up to 50 ml. 20 ml of the solution and 5 ml of glass-distilled water were added to a glass test tube. Solution was shaken vigorously for 1 min and allowed to separate into two phases. Glass scintillation vials were weighted with analytical balance. The lower phase of the solution was transferred to the glass scintillation vials and dried under gentle air. The vials were weighed again using an analytical balance. Calculations were performed to analyze the fecal lipid content in each mouse.

RNA-seq

Total RNA from frozen livers of three biological replicates was extracted using TRIzol reagent (Invitrogen, Carlsbad, CA). Library construction and sequencing were performed by the UTSW Genomics and Microarray Core Facility, and detailed procedures can be found from the following website: https://microarray.swmed.edu/. Canonical pathways analysis was performed by Ingenuity® Pathway Analysis (IPA®) (Qiagen, Hilden, Germany). RNA-seq data have been deposited at GEO under accession number GEO####.

Data analysis

Statistical analysis was performed using GraphPad Prism software (GraphPad Software, San Diego, CA). Experimental values are depicted as the mean ± SEM. Statistical significance between two groups was determined using two-tailed Student's t-test. One-way ANOVA was applied for multi-group comparisons. P values of less than 0.05 were considered to be significant.

Protein preparation

All constructs were generated using a standard PCR-based cloning strategy. Full-length LCMT-1 or PPM1 were cloned in pET15b vector (Invitrogen) and were overexpressed at 16 degree in *E. coli* strain BL21(DE3). The soluble fraction of the *E. coli* cell lysate was purified by the Ni-NTA resin (QIAGEN) to homogeneity and further fractionated by ion-exchange chromatography (Source 15Q, Amersham).

ITC

Binding of SAM and SAH to LCMT-1 and PPM1 were assessed by ITC using a Small-Volume Isothermal Titration Calorimetry (Microcal ITC-200; GE Healthcare). LCMT-1 or PPM1 protein samples were dialyzed extensively against ITC buffer [50 mM Tris·HCl (pH 8.0), 50 mM NaCl] and degassed in a vacuum. SAM and SAH also were dissolved in ITC buffer. The binding experiments were performed at 25- ℃. Titrations comprised 20 injections of SAM or SAH. The initial data point was deleted routinely to allow for diffusion of ligand/receptor across the needle tip during the equilibration period. ITC-binding isotherms were analyzed using a simple single-binding-site model with the ITC data analysis software provided by the UTSW Macromolecular Biophysics Resource Core Facility.

Methylation assay and High-throughput screen (HTS)

PP2A methylation assay was carried out in a mixture of reaction buffer (10 mM Tris-HCl, pH 8.0, 150 mM NaCl, 50 μM $MnCl_2$, 5 mM DTT, 0.01% BSA), 2 μM SAM, and 0.6 μM PP2A core enzyme. The reaction was initiated by the addition of 0.2 μM LCMT-1. After 80 min at room temperature, the reaction was stopped by the addition of 0.2% formic acid.

For the HTS mock plate, PP2A methylation was carried out in a 384-well format using the assay described above with the first and the last columns of the plate reserved for the negative control DMSO. Columns 2 and 23 were used for a neutral control (DMSO alone). The reaction was initiated by mixing 40 μl reaction mix (reaction buffer + PP2A + LCMT-1, as described above). After the plate was incubated at room temperature for 80 min,

the reaction was quenched by the addiction of 40 µl of 0.2% formic acid. After quenching the reaction, samples from all plates were read using the RapidFire 300. These results were expressed as an extent of reaction (Product/(Product + Substrate), P/(P+S)), loaded into GeneData's Screener software, normalized, and scaled such that 0 represents no effect, values above 0 represent an activation of enzyme activity, and values less than 0 represent inhibition of enzyme activity.

For the HTS, The University of Texas Southwestern chemical library used for this screen consisted of 11k compounds from the HTS core all of which passed 48 structure-based filters that are designed to remove compounds with undesirable properties (*e.g.* reactive and/or undesirable functional groups) and that satisfy a relaxed version of Lipinski's rules for good oral bioavailability.

Acknowledgement

There are many people that have earned my gratitude for their contribution to my time in graduate school. More specifically, I would like to thank four groups of people, without whom this thesis would not have been possible: my thesis committee members, my lab mates, my collaborators, and my family.

First, I am indebted to my thesis advisor, Dr. Benjamin Tu. Since my first day in the lab, Ben believed in me like nobody else and gave me endless support. Under his supervision, I learned how to define a research problem, find a solution to it, and finally publish the results. Besides my advisor, I would like to thank the rest of my dissertation committee members (Dr. Jennifer Kohler, Dr. Deepak Nijhawan, and Dr. Hongtao Yu) for their great support and invaluable advice.

I would like to thank my lab mates for their continued support. This dissertation would not have been possible without the intellectual contribution of two lab alumni, Gunes Bender and Zhiguang Huang. Moreover, I am thankful to Yun Wang for her contribution to PP2A project, and to Sandi Jo Terpack and Abigail Plec for their contribution to ACSS2 projects. I would also like to thank my other lab mates that include Benjamin Sutter, Cunqi Ye, Floortje Van De Poll, Kuanqing Liu, Madeline Milligan, Wen-Chuan Hsieh, Yu-San Yang, and Zane Johnson for making my experience in the lab and graduate school exciting and fun.

Thanks are also due to my collaborators. I would like to thank Dr. Sarah Comerford, Dr. Robert Hammer, Dr. Joyce Repa, Dr. Sam Wang, and Dr. Suntrea Hammer for their collaboration and contribution to ACSS2 projects. I would like to thank Dr. Bruce Posner, director of the UTSW high-throughput screening Core Facility for helping with the screening of LCMT-1 inhibitor. I also extend my gratitude to Dr. Yongna Xing at University of Wisconsin Madison for her help with PP2A protein preparation.

Last but not least, I would like to express my deepest gratitude to my family and friends. This dissertation would not have been possible without their warm love, continued patience, and endless support.

Bibliography

Aguirre, A. J., Bardeesy, N., Sinha, M., Lopez, L., Tuveson, D. A., Horner, J., ... & DePinho, R. A. (2003). Activated Kras and Ink4a/Arf deficiency cooperate to produce metastatic pancreatic ductal adenocarcinoma. *Genes & development*, *17*(24), 3112-3126.

Bar-Peled, L., Chantranupong, L., Cherniack, A. D., Chen, W. W., Ottina, K. A., Grabiner, B. C., ... & Sabatini, D. M. (2013). A Tumor suppressor complex with GAP activity for the Rag GTPases that signal amino acid sufficiency to mTORC1. *Science*, *340*(6136), 1100-1106.

Beigneux, A. P., Kosinski, C., Gavino, B., Horton, J. D., Skarnes, W. C., & Young, S. G. (2004). ATP-citrate lyase deficiency in the mouse. *Journal of Biological Chemistry*, *279*(10), 9557-9564.

Berg, P. (1956). *Acyl adenylates: an enzymatic mechanism of acetate activation*. American Society for Biochemistry and Molecular Biology.

Blücher, C., & Stadler, S. C. (2017). Obesity and Breast Cancer: Current Insights on the Role of Fatty Acids and Lipid Metabolism in Promoting Breast Cancer Growth and Progression. *Frontiers in endocrinology*, *8*.

Boer, V. M., Amini, S., & Botstein, D. (2008). Influence of genotype and nutrition on survival and metabolism of starving yeast. *Proceedings of the National Academy of Sciences*, *105*(19), 6930-6935.

Cabreiro, F., Au, C., Leung, K. Y., Vergara-Irigaray, N., Cochemé, H. M., Noori, T., ... & Gems, D. (2013). Metformin retards aging in C. elegans by altering microbial folate and methionine metabolism. *Cell*, *153*(1), 228-239.

Cai, L., Sutter, B. M., Li, B., & Tu, B. P. (2011). Acetyl-CoA induces cell growth and proliferation by promoting the acetylation of histones at growth genes. *Molecular cell*, *42*(4), 426-437.

Caudill, M. A., Wang, J. C., Melnyk, S., Pogribny, I. P., Jernigan, S., Collins, M. D., ... & James, S. J. (2001). Intracellular S-adenosylhomocysteine concentrations predict global DNA hypomethylation in tissues of methyl-deficient cystathionine β-synthase heterozygous mice. *The Journal of nutrition*, *131*(11), 2811-2818.

Chin, H. G., Patnaik, D., Esteve, P. O., Jacobsen, S. E., & Pradhan, S. (2006). Catalytic properties and kinetic mechanism of human recombinant Lys-9 histone H3 methyltransferase SUV39H1: participation of the chromodomain in enzymatic catalysis. *Biochemistry*, *45*(10), 3272-3284.

Cohen, J. C., Horton, J. D., & Hobbs, H. H. (2011). Human fatty liver disease: old questions and new insights. *Science*, *332*(6037), 1519-1523.

Comerford, S. A., Huang, Z., Du, X., Wang, Y., Cai, L., Witkiewicz, A. K., ... & Horton, J. D. (2014). Acetate dependence of tumors. *Cell*, *159*(7), 1591-1602.

D'Aquila, T., Hung, Y. H., Carreiro, A., & Buhman, K. K. (2016). Recent discoveries on absorption of dietary fat: Presence, synthesis, and metabolism of cytoplasmic lipid droplets within enterocytes. *Biochimica et Biophysica Acta (BBA)-Molecular and Cell Biology of Lipids*, *1861*(8), 730-747.

Distler, M., Aust, D., Weitz, J., Pilarsky, C., & Grützmann, R. (2014). Precursor lesions for sporadic pancreatic cancer: PanIN, IPMN, and MCN. *BioMed research international*, *2014*.

Fellner, T., Lackner, D. H., Hombauer, H., Piribauer, P., Mudrak, I., Zaragoza, K., ... & Ogris, E. (2003). A novel and essential mechanism determining specificity and activity of protein phosphatase 2A (PP2A) in vivo. *Genes & development*, *17*(17), 2138-2150.

Glaudemans, A. W., Enting, R. H., Heesters, M. A., Dierckx, R. A., van Rheenen, R. W., Walenkamp, A. M., & Slart, R. H. (2013). Value of 11 C-methionine PET in imaging brain tumours and metastases. *European journal of nuclear medicine and molecular imaging*, *40*(4), 615-635.

Grandison, R. C., Piper, M. D., & Partridge, L. (2009). Amino-acid imbalance explains extension of lifespan by dietary restriction in Drosophila. *Nature*, *462*(7276), 1061.

Grassi, I., Nanni, C., Allegri, V., Morigi, J. J., Montini, G. C., Castellucci, P., & Fanti, S. (2012). The clinical use of PET with 11C-acetate. *American journal of nuclear medicine and molecular imaging*, *2*(1), 33.

Incio, J., Liu, H., Suboj, P., Chin, S. M., Chen, I. X., Pinter, M., ... & Babykutty, S. (2016). Obesity-induced inflammation and desmoplasia promote pancreatic cancer progression and resistance to chemotherapy. *Cancer discovery*, *6*(8), 852-869.

Jackson, V., Shires, A., Chalkley, R., & Granner, D. K. (1975). Studies on highly metabolically active acetylation and phosphorylation of histones. *Journal of Biological Chemistry*, *250*(13), 4856-4863.

Ji, L., Nishizaki, M., Gao, B., Burbee, D., Kondo, M., Kamibayashi, C., ... & Lerman, M. I. (2002). Expression of several genes in the human chromosome 3p21. 3 homozygous deletion region by an adenovirus vector results in tumor suppressor activities in vitro and in vivo. *Cancer research*, *62*(9), 2715-2720.

Jones, M. E., Lipmann, F., Hilz, H., & Lynen, F. (1953). On the enzymatic mechanism of coenzyme A acetylation with adenosine triphosphate and acetate 1. *Journal of the American Chemical Society*, *75*(13), 3285-3286.

Kalhor, H. R., Luk, K., Ramos, A., Zobel-Thropp, P., & Clarke, S. (2001). Protein phosphatase methyltransferase 1 (Ppm1p) is the sole activity responsible for modification of the major forms of protein phosphatase 2A in yeast. *Archives of biochemistry and biophysics*, *395*(2), 239-245.

Kawaguchi, Y., Cooper, B., Gannon, M., Ray, M., MacDonald, R. J., & Wright, C. V. (2002). The role of the transcriptional regulator Ptf1a in converting intestinal to pancreatic progenitors. *Nature genetics*, *32*(1), 128.

Laxman, S., Sutter, B. M., & Tu, B. P. (2014). Methionine is a signal of amino acid sufficiency that inhibits autophagy through the methylation of PP2A. *Autophagy*, *10*(2), 386-387.

Lee, B. C., Kaya, A., Ma, S., Kim, G., Gerashchenko, M. V., Yim, S. H., ... & Gladyshev, V. N. (2014). Methionine restriction extends lifespan of Drosophila melanogaster under conditions of low amino-acid status. *Nature communications*, *5*, 3592.

Lee, J., & Stock, J. (1993). Protein phosphatase 2A catalytic subunit is methyl-esterified at its carboxyl terminus by a novel methyltransferase. *Journal of Biological Chemistry*, *268*(26), 19192-19195.

Li, J., Wang, F., Haraldson, K., Protopopov, A., Duh, F. M., Geil, L., ... & Kashuba, V. I. (2004). Functional characterization of the candidate tumor suppressor gene NPRL2/G21 located in 3p21. 3C. *Cancer research*, *64*(18), 6438-6443.

Ling, J., Morley, S. J., & Traugh, J. A. (2005). Inhibition of cap-dependent translation via phosphorylation of eIF4G by protein kinase Pak2. *The EMBO journal*, *24*(23), 4094-4105.

Luong, A., Hannah, V. C., Brown, M. S., & Goldstein, J. L. (2000). Molecular characterization of human acetyl-CoA synthetase, an enzyme regulated by sterol regulatory element-binding proteins. *Journal of Biological Chemistry*, *275*(34), 26458-26466.

Nagai, S., Davis, R. E., Mattei, P. J., Eagen, K. P., & Kornberg, R. D. (2017). Chromatin potentiates transcription. *Proceedings of the National Academy of Sciences*, *114*(7), 1536-1541.

Neklesa, T. K., & Davis, R. W. (2009). A genome-wide screen for regulators of TORC1 in response to amino acid starvation reveals a conserved Npr2/3 complex. *PLoS genetics*, *5*(6), e1000515.

Okumura, T., Ohuchida, K., Sada, M., Abe, T., Endo, S., Koikawa, K., ... & Nakata, K. (2017). Extra-pancreatic invasion induces lipolytic and fibrotic changes in the adipose microenvironment, with released fatty acids enhancing the invasiveness of pancreatic cancer cells. *Oncotarget*, *8*(11), 18280.

Oldfield, L. E., Connor, A. A., & Gallinger, S. (2017). Molecular events in the natural history of pancreatic cancer. *Trends in cancer*, *3*(5), 336-346.

Pallas, D. C., Shahrik, L. K., Martin, B. L., Jaspers, S., Miller, T. B., Brautigan, D. L., & Roberts, T. M. (1990). Polyoma small and middle T antigens and SV40 small t antigen form stable complexes with protein phosphatase 2A. *Cell*, *60*(1), 167-176.

Panchaud, N., P đi-Gulli, M. P., & De Virgilio, C. (2013). Amino acid deprivation inhibits TORC1 through a GTPase-activating protein complex for the Rag family GTPase Gtr1. *Sci. Signal.*, *6*(277), ra42-ra42.

Patnaik, D., Chin, H. G., Esteve, P. O., Benner, J., Jacobsen, S. E., & Pradhan, S. (2004). Substrate specificity and kinetic mechanism of mammalian G9a histone H3 methyltransferase. *Journal of Biological Chemistry*, *279*(51), 53248-53258.

Psychogios, N., Hau, D. D., Peng, J., Guo, A. C., Mandal, R., Bouatra, S., ... & Young, N. (2011). The human serum metabolome. *PloS one*, *6*(2), e16957.

Sakakibara, I., Fujino, T., Ishii, M., Tanaka, T., Shimosawa, T., Miura, S., ... & Iwasaki, S. (2009). Fasting-induced hypothermia and reduced energy production in mice lacking acetyl-CoA synthetase 2. *Cell metabolism*, *9*(2), 191-202.

Schmittgen, T. D., & Livak, K. J. (2008). Analyzing real-time PCR data by the comparative C T method. *Nature protocols*, *3*(6), 1101.

Seshacharyulu, P., Pandey, P., Datta, K., & Batra, S. K. (2013). Phosphatase: PP2A structural importance, regulation and its aberrant expression in cancer. *Cancer letters*, *335*(1), 9-18.

Shi, L., & Tu, B. P. (2015). Acetyl-CoA and the regulation of metabolism: mechanisms and consequences. *Current opinion in cell biology*, *33*, 125-131.

Shi, Y. (2009). Serine/threonine phosphatases: mechanism through structure. *Cell*, *139*(3), 468-484.

Singhal, T., Narayanan, T. K., Jacobs, M. P., Bal, C., & Mantil, J. C. (2012). 11C-methionine PET for grading and prognostication in gliomas: a comparison study with

18F-FDG PET and contrast enhancement on MRI. *Journal of Nuclear Medicine*, *53*(11), 1709.

Sonenberg, N., & Hinnebusch, A. G. (2009). Regulation of translation initiation in eukaryotes: mechanisms and biological targets. *Cell*, *136*(4), 731-745.

Sontag, E., Hladik, C., Montgomery, L., Luangpirom, A., Mudrak, I., Ogris, E., & White III, C. L. (2004). Downregulation of protein phosphatase 2A carboxyl methylation and methyltransferase may contribute to Alzheimer disease pathogenesis. *Journal of Neuropathology & Experimental Neurology*, *63*(10), 1080-1091.

Srere, P. A. (1959). The citrate cleavage enzyme. *J. biol. Chem*, *234*, 2544-2547.

Stanevich, V., Jiang, L., Satyshur, K. A., Li, Y., Jeffrey, P. D., Li, Z., ... & Xing, Y. (2011). The structural basis for tight control of PP2A methylation and function by LCMT-1. *Molecular cell*, *41*(3), 331-342.

Stanevich, V., Zheng, A., Guo, F., Jiang, L., Wlodarchak, N., & Xing, Y. (2014). Mechanisms of the scaffold subunit in facilitating protein phosphatase 2A methylation. *PloS one*, *9*(1), e86955.

Storch, J., & Corsico, B. (2008). The emerging functions and mechanisms of mammalian fatty acid–binding proteins. *Annu. Rev. Nutr.*, *28*, 73-95.

Sutter, B. M., Wu, X., Laxman, S., & Tu, B. P. (2013). Methionine inhibits autophagy and promotes growth by inducing the SAM-responsive methylation of PP2A. *Cell*, *154*(2), 403-415.

Ulanovskaya, O. A., Zuhl, A. M., & Cravatt, B. F. (2013). NNMT promotes epigenetic remodeling in cancer by creating a metabolic methylation sink. *Nature chemical biology*, *9*(5), 300.

Vafai, S. B., & Stock, J. B. (2002). Protein phosphatase 2A methylation: a link between elevated plasma homocysteine and Alzheimer's Disease. *FEBS letters*, *518*(1-3), 1-4.

Varghese, F., Bukhari, A. B., Malhotra, R., & De, A. (2014). IHC Profiler: an open source plugin for the quantitative evaluation and automated scoring of immunohistochemistry images of human tissue samples. *PloS one*, *9*(5), e96801.

Waterborg, J. H. (2002). Dynamics of histone acetylation in vivo. A function for acetylation turnover?. *Biochemistry and cell biology*, *80*(3), 363-378.

Wei, H., Ashby, D. G., Moreno, C. S., Ogris, E., Yeong, F. M., Corbett, A. H., & Pallas, D. C. (2000). Carboxy-methylation of the PP2A catalytic subunit in Saccharomyces

cerevisiae is required for efficient interaction with the B-type subunits, Cdc55p and Rts1p. *Journal of Biological Chemistry*.

Wu, J., Tolstykh, T., Lee, J., Boyd, K., Stock, J. B., & Broach, J. R. (2000). Carboxyl methylation of the phosphoprotein phosphatase 2A catalytic subunit promotes its functional association with regulatory subunits in vivo. *The EMBO journal*, *19*(21), 5672-5681.

Wu, X., & Tu, B. P. (2011). Selective regulation of autophagy by the Iml1-Npr2-Npr3 complex in the absence of nitrogen starvation. *Molecular biology of the cell*, *22*(21), 4124-4133.

Xie, H. O. N. G. Y. I. N. G., & Clarke, S. (1993). Methyl esterification of C-terminal leucine residues in cytosolic 36-kDa polypeptides of bovine brain. A novel eucaryotic protein carboxyl methylation reaction. *Journal of Biological Chemistry*, *268*(18), 13364-13371.

Xu, Y., Xing, Y., Chen, Y., Chao, Y., Lin, Z., Fan, E., ... & Shi, Y. (2006). Structure of the protein phosphatase 2A holoenzyme. *Cell*, *127*(6), 1239-1251.

Yen, C. L. E., Stone, S. J., Koliwad, S., Harris, C., & Farese, R. V. (2008). Thematic review series: glycerolipids. DGAT enzymes and triacylglycerol biosynthesis. *Journal of lipid research*, *49*(11), 2283-2301.